Benchmarking Pt and Pt-lanthanide sputtered thin films for oxygen electroreduction
fabrication and rotating disk electrode measurements

Zamburlini, Eleonora; Jensen, Kim Degn; Stephens, Ifan E.L.; Chorkendorff, Ib; Escribano, Maria Escudero

Published in:
Electrochimica Acta

Link to article, DOI:
10.1016/j.electacta.2017.06.146

Publication date:
2017

Document Version
Peer reviewed version

Benchmarking Pt and Pt-lanthanide sputtered thin films for oxygen electroreduction: fabrication and rotating disk electrode measurements

Eleonora Zamburlini[a], Kim D. Jensen[a], Ifan E. L. Stephens[a], Ib Chorkendorff[a], and María Escudero-Escribano[a,b*]

[a] Section for Surface Physics and Catalysis, Department of Physics, Building 312, Technical University of Denmark (DTU), DK-2800 Kgs. Lyngby, Denmark

[b]Department of Chemistry, University of Copenhagen, DK-2100, Copenhagen, Denmark

[*]Corresponding author: María Escudero-Escribano

e-mail: maria.escudero@chem.ku.dk

Abstract

Platinum-lanthanide alloys are very promising as active and stable catalysts for the oxygen reduction reaction (ORR) in low-temperature fuel cells. We have fabricated Pt and Pt_5Gd metallic thin films *via* (co-)sputtering deposition in an ultra-high vacuum (UHV) chamber. The electrochemical ORR activity, stability, as-well as chemical composition and crystallographic structure of Pt_5Gd thin film catalysts have been investigated using a combination of electrochemical measurements, X-ray photoemission spectroscopy (XPS) and X-ray diffraction (XRD) techniques. We describe the measurement procedures, with the aim of benchmarking electrochemical characterization of Pt-based thin film catalysts for ORR. Pt_5Gd thin films present an activity enhancement by a factor of 4.5 and 2.5 over polycrystalline Pt and Pt thin films, respectively.

Keywords:

Electrocatalysis, Oxygen Reduction Reaction, Rotating Disk Electrode, Pt-Alloys, Sputtering, Thin Films, Benchmarking

1. Introduction

Proton exchange membrane fuel cells (PEMFCs) are one of the most promising technologies for potentially zero emission power conversion [1]. They are suitable for both automotive and stationary applications, and will likely play an important role in future sustainable energy schemes [2–5]. However, the high costs of PEMFCs, and specifically of the Pt-based electrocatalysts, constitute a major obstacle for a commercially competitive reality [6]. Currently, a state-of-the-art PEMFC require a Pt loading of 0.25 g_{Pt}/kW, of which 0.2 mg_{Pt}/cm^2 are required at the cathode, where the oxygen reduction reaction (ORR) takes place [3,6]:

$$O_2 + 4H^+ + 4e^- \rightarrow 2H_2O \qquad (1)$$

The slow kinetics of the ORR causes significant potential losses (overpotentials). As such, this is the limiting reaction in PEMFCs. Using current technologies, the amount of Pt available is too scarce to ensure a widespread implementation of PEMFCs [7]. In order to reduce the Pt loading at the cathode, we need to develop new electrocatalysts with enhanced activity and improved long-term stability under realistic operating conditions [2,7–9]. It is important to note that an order of magnitude decrease in the amount of Pt employed at the cathode of a PEMFC would result in a Pt group metal loading equal to that of advanced catalytic converters for automotive vehicles in terms of Pt usage [3].

The ORR on pure Pt surfaces has been studied extensively. In 0.1 M $HClO_4$, the ORR activity follows the order Pt(100)<Pt(111)<Pt(110) [10]. Moreover, defects such as steps [11–14] and concave defects [15] seem to enhance oxygen reduction. It is clear that the ORR is structure-sensitive. Therefore, modifying the surface structure can enhance the catalytic activity, selectivity and stability [16].

The OH binding energy governs the ORR activity on Pt-based catalysts [17]. Other indirect descriptors influence the OH binding energy, such as the lattice parameter [8,18,19] the d-band center [9,17] and the generalized coordination number [15]. The ORR activity of Pt can be enhanced by modification of the geometric structure (atomic ensemble effects) [20] and/or alteration of the electronic properties of the surface atoms (electronic effects). The latter can be tuned by alloying Pt with other metals [7,9,21,22]. The desired effect of alloying is to weaken the OH binding energy [9,17] by means of strain [8,23,24] and/or ligand effects [25,26].

During the last few decades, catalyst developers have intensively studied alloys of Pt and late transition metals for the ORR: Pt-Ni, Pt-Cu, Pt-Fe and Pt-Co alloys all present an enhanced activity over pure Pt [9,18,21,23,25,27–29]. Several studies have shown that a Pt overlayer is formed after immersion in

acidic electrolyte [22,28]. The composition and stoichiometry of the alloy influence the Pt overlayer structure, and therefore the activity and stability [22,30–33]. Nonetheless, these catalysts often tend to degrade via dealloying under operating fuel cell conditions [6,34,35]. Appropriate synthesis conditions can lead to exceptional stability during short-term accelerated degradation tests [36–40]. Even so, it is an open question whether they can survive long-term stability tests [41] and whether the impressive enhancement factors obtained during ideal rotating disk electrode (RDE) experiments can be translated to fuel cells [42].

Recent studies have demonstrated that it is possible to obtain a remarkable improvement in activity by alloying Pt with early transition metals and rare earths [8,43,44]. Our studies on polycrystalline Pt-early transition metal and Pt-lanthanide alloys show up to a 6-fold improvement in activity at 0.9 V *vs.* RHE over polycrystalline Pt [8,43–46]. Moreover, the lanthanide alloys have a very negative enthalpy of formation, which may stabilize them kinetically against degradation *via* dealloying [41,47,48]. Nevertheless, rare earths such as Gd are thermodynamically unstable towards dissolution in acid; their kinetic stability is contingent on the robustness of the Pt overlayers ability to protect the alloys from further losses and increase their stability [8,49].

We synthesized mass-selected nanoparticles of Pt-rare earth alloys using a magnetron nanoparticle source, which demonstrated excellent catalytic properties towards ORR, with a mass activity for Pt_xGd nanoparticles of 3.6 A/mg_{Pt} [49]. At the same time, our extended X-ray absorption fine structure (EXAFS) experiments showed that the nanoparticles are under compressive strain [49,50] the ORR activity increasing as the bulk compressive strain decreased [49]. In order to mass produce these catalysts and insert them in real PEMFCs, a chemical synthesis method has to be implemented. However, it is very challenging to synthesize Pt-lanthanide alloys chemically, to the most part due to the high oxygen affinity of lanthanides [51].

Pt and Pt-late transition metal catalysts in thin film form have been fabricated successfully [31,52–54]. In the field of fuel cells, nanostructured thin films (NSTFs) and mesostructured thin films of Pt [54] and Pt-Ni [31,55] have been fabricated and successfully tested for activity and stability towards ORR. The Pt loading have been optimized, and these catalysts demonstrated higher activity of the alloys as compared to pure Pt films. *Morimoto and co-workers* showed that atomic layer deposition (ALD) can be successfully employed to produce Pt electrodes on SiO_2 substrates for testing on MEAs [56]. More recently, *Schmidt and co-workers* investigated the influence of the growth mechanism on the surface

structure of thin films fabricated by pulsed laser deposition (PLD), demonstrating that strain can enhance the ORR activity [57,58]. *Kim and co-workers* fabricated nanoparticulate thin films of alloys of Pt-late transition metals together with Pt-Y and Pt-La for ORR using magnetron sputtering [59–61]. Their results show that Pt_3Y thin films presented enhanced activity and stability in comparison to the rest of the Pt-alloy thin films tested.

Herein we present a method for fabrication of thin films of Pt and Pt-lanthanide alloys *via* co-sputtering, together with the detailed procedures to measure the electrochemical activity and stability towards ORR, using a rotating ring-disk electrode (RRDE) setup. This article reports, for the first time, the fabrication, characterization and electrochemical performance of thin films of Pt-Gd alloys for the ORR.

The sputtering technique consists of a beam of ionized Ar hitting the target and knocking out atoms. Some of the ejected material will then deposit on the designated substrate. This technique has already been used for the preparation of catalysts in electrochemistry [62–64]. The main advantage of thin films is that they can cover large areas and can be inexpensively mass-produced at a reasonable rate. For a model study of the electrochemical properties, it is much easier to work on fabricated thin films samples compared to expensive polycrystalline samples, which require Ar sputter cleaning treatment in UHV before the electrochemical [8]. Thin films make it easier to test different stoichiometry of Pt alloys, in order to optimize the ratio and minimize the Pt loading.

The focus of this paper is to investigate the ORR activity and stability of model sputtered Pt and Pt_5Gd thin films. We aim to give key recommendations in order to be able to fabricate these Pt-based thin films and carry out the electrochemical measurements in a reliable way, relevant for PEMFC devices.

2. Experimental

2.1. Sample preparation

Pt_5Gd and Pt thin films were prepared by sputter deposition in UHV compatible system from AJA. The chamber constitutes of a load lock that can be pumped down before transferring samples into the main chamber, a transferring arm, and the main chamber, which can be pumped down to a base pressure of 10^{-9} mTorr. The load lock can be vented by flushing with Ar (purity 5.0). The chamber can contain up

to 9 targets of which three can be used simultaneously. The distance between substrate and target is approximately 10 to 15 cm. The substrate holder is cooled down by a water cooler.

The main chamber is equipped with a quartz crystal microbalance (QCM) to measure the deposition rate, a shutter that can be placed in front of the substrates to prevent deposition and a heating wire, for substrate heating up to 850 °C. A schematic of the co-sputtering process is provided in Figure 1. Additionally, oxygen can be leaked into the chamber to fabricate oxides thin films *e.g.* of MnO_x catalysts for oxygen evolution [64]. The substrate consisted of Ar sputter cleaned and polished glassy carbon (GC) disks of 5 mm diameter from HTW Hochtemperatur-Werkstoffe.

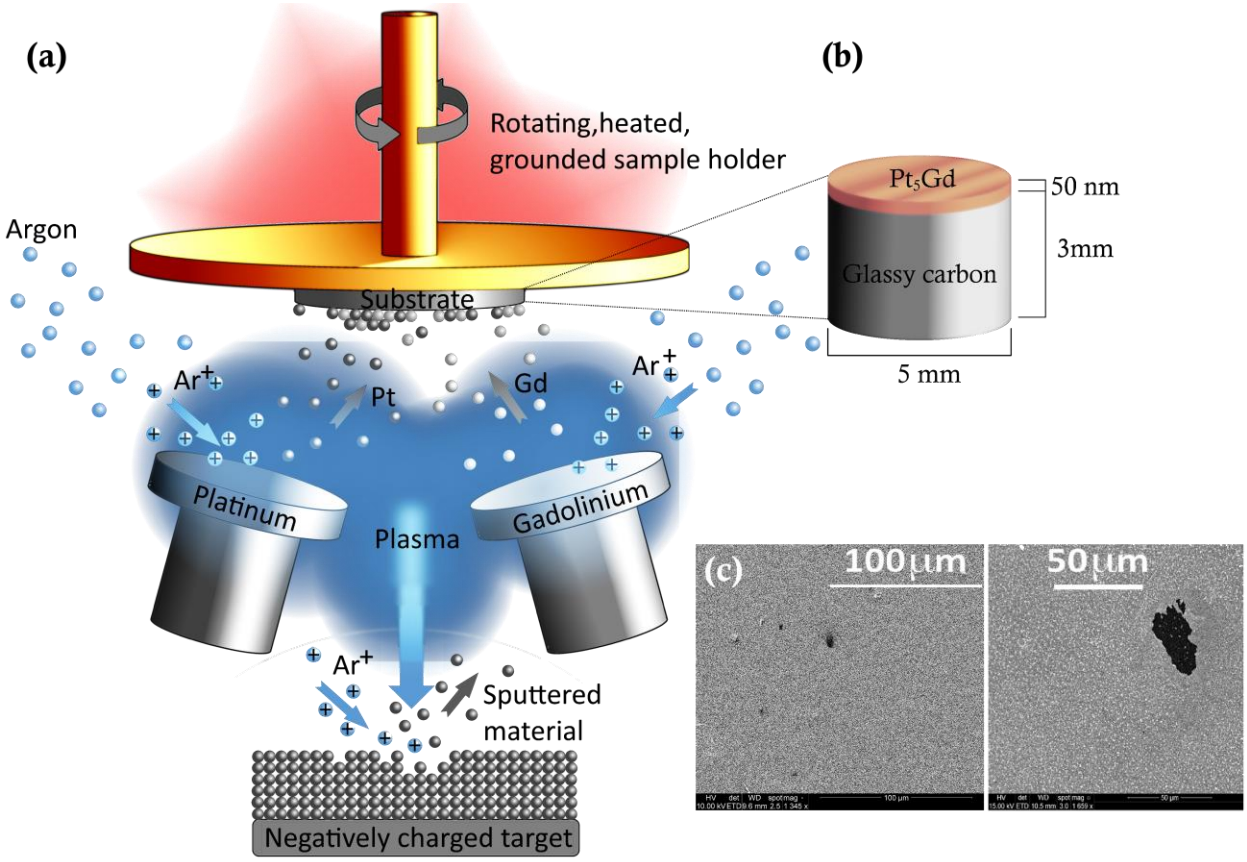

Figure 1. (a) Schematic of the sputter deposition process. Ar gas is ionized to plasma to form Ar^+ (blue). A negative bias is applied on the target material (gray), which causes the Ar^+ to bombard the surface and knock atoms loose. Some of the target atoms then deposit on the grounded substrate. Magnets confine the plasma near the targets; **(b)** Schematic representation of the Pt_5Gd thin film on top of the glassy carbon disk; **(c)** Scanning electron microscope (SEM) image of dealloyment due to the presence of oxygen in a Pt_5Gd thin film.

A GC square plate (1 cm^2) with polished top side was also loaded in the chamber for each deposition, to be used for XRD and XPS testing. The polishing procedure included a polishing step using a polishing disk and diamond paste from Struers and a sonicating step. The polishing step consisted of mounting the disk on a rotating support; the paste was spread on it and the glassy carbon surface was put in contact for 30 to 60 s. The sonicating step involved three cycles of sonication, where one "sonication cycle" constituted 10 min sonication in water and 10 min sonication in isopropanol. The glassy carbons were subsequently dried with Ar. The cleanliness of the surface is crucial for a good thin film deposition since it minimizes the contamination and lowers the roughness.

Because of the high oxygen affinity of the lanthanides, they will react with minimal amounts of oxygen present in the chamber and form oxides. Such oxide formation will compromise the electrochemical measurement, since the alloy will not form, and when immersed in the acidic environment for the electrochemical testing, the lanthanide-oxides will leach out of the film, which will dealloy (Figure 1c). Therefore, it is crucial to develop deposition routines that minimize the amount of oxygen in the UHV system. Herein we transcribe the procedure for removing the oxygen traces from the UHV chamber in an efficient and reproducible way:

1) The glassy carbon substrates were loaded in the load lock. When the load lock pressure was at least 10^{-7} mTorr, they were then transferred to the main chamber.
2) The substrates were heated up to 200 °C to make sure every water trace on them evaporated.
3) Ar sputtering on the substrates was performed for 45 min to eliminate all contamination from the surface.
4) The shutter was positioned in front of the substrates to prevent deposition, while Ti was sputtered in the chamber for 30 to 45 min, acting as a Ti sublimation pump, and leading to the removal of oxygen.
5) The chamber was then pumped down for 10 to 12 h until reaching a base pressure of 10^{-9} mTorr.

The samples were deposited at 4 mbar with a 50 sccm Ar flow. For the scope of this article all the reported results are related to our standard thin film samples:

- Pure Pt sample of 40 nm deposited at 300 °C.
- Pt_5Gd sample of 50 nm deposited at 300 °C.

The Pt power for this deposition was 180 W, while the Gd power was between 25 and 30 W, adjusted before every set of deposition accordingly with a measurement taken with the QCM. After deposition, the temperature was kept at 300 °C for 10 min. The samples were cooled in the chamber for 2 to 3 h.

2.2. Electrochemical characterisation

All electrochemical measurements were performed in a cell using an RRDE setup. The data have been Ohmic drop corrected and presented *vs.* the reversible hydrogen electrode (RHE). Before every set of electrochemical measurements, all the glassware was cleaned in piranha solution (98 % H_2SO_4 (Merck, Emsure) and 30 % H_2O_2 (Merck, Emsure), 3:1 V/V) for at least 24 h. Several different cleaning procedures can be found in the literature [65]. We use the piranha cleaning as we find it is most effective in removing traces of organic contamination and ensure reproducible measurements on Pt-based well-defined electrodes [8]. The glassware was then rinsed with 18.2 MΩ cm Millipore water at least 5 times and sonicated for 30 min at 70 °C to remove all traces of the cleaning solution. The electrochemical cell was rinsed from piranha 5 times and then heated using an heating jacket to 90 °C. The temperature was maintained for some hours, and the water inside the cell was changed 5 to 6 times.

The electrochemical cell is shown in Figure 2, and consists of:

- Two Pt wires (Chempur 99.9 %, 0.5 mm diameter). The Pt wires fit into the side holes, one of which is used as counter electrode.
- A $Hg_{(l)}|HgSO_{4(g)}$ reference electrode (Schott Instruments), fitted in a separate compartment ending with a Luggin capillary, which terminates as close as possible to the sample surface, in order to minimize the Ohmic drop from the electrolyte resistance. All the potentials in this study all refer to that of the RHE.
- A gas inlet placed on the side of the cell, which allows saturating the cell with gasses without inserting tubes directly into the electrolyte.
- An external glass jacket, which can be connected to a water heater for temperature control.

The electrolyte consisted of 0.1 M $HClO_4$ prepared from 70 % $HClO_4$ (Merck Suprapur, 99.99 % purity) and 18.2 MΩ cm Millipore water. Prior to the measurements, the cell was heated repeatedly to 90 °C using the water heater and rinsed 5 times with Millipore water, letting 20 min passing between

each rinse. During one of the rinsing, bubbling N_2 through the glass bubbler helps eliminate eventual residues (*e.g.* sulphate anions from the piranha solution).

The samples were mounted on a rotating disk Teflon tip using Teflon U-cups. The tips and the U-cups have been purchased from Pine Instruments and have also been previously cleaned in piranha solution. To make the mounting as clean as possible, the samples were placed face down on a polypropylene film (from Chemoplex) previously sonicated for 20 min at 50 °C in Millipore water. Before mounting the sample on the rotator, the tip was rinsed with Millipore water [66,67].

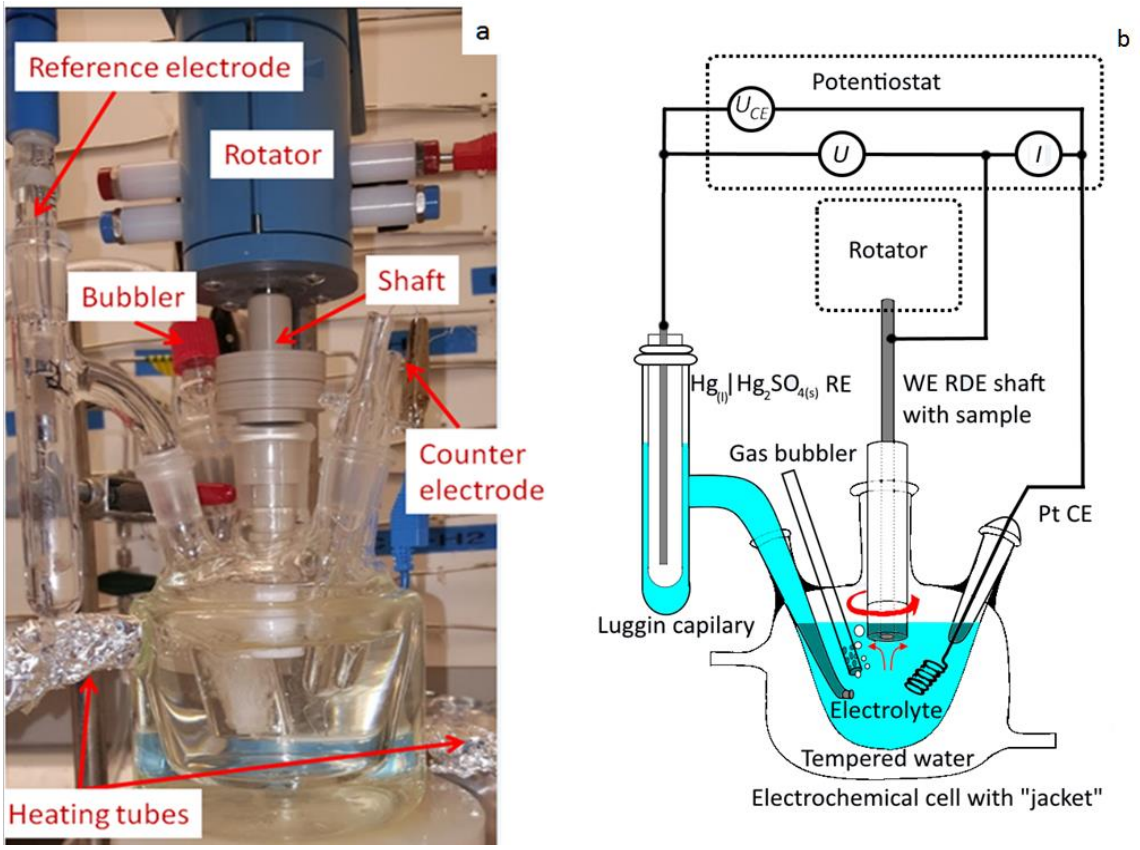

Figure 2. (a) Photo of the electrochemical cell and **(b)** schematic representation of the cell. The main parts are visible: the Pt wire (counter electrode), the Luggin capillary, the bubbler, the heating jackets and the rotator where the shaft holding the RDE tip is mounted.

The electrochemical measurements were performed using a VMP2 multi-channel potentiostat (Bio-Logic Instruments), controlled from a computer using EC-Lab software. All the gasses used were supplied by AGA with instrument 5.0 purities for Ar, N_2 and O_2 gasses, instrument 4.5 for the H_2 gas and instrument 3.7 for the CO gas.

All experiments were performed at room temperature (23 °C) and maintained with the heated water jacket of the cell (see Figure 2). Before measuring the sputtered Pt-based thin films, we performed a test measurement with polycrystalline Pt (purchased from Pine, purity 99.99 %), to check the cleanliness of the cell. Before the measurement, the polycrystalline Pt electrode was flame annealed for 5 min, using a LPG torch (Proxxon), then cooled down in a glass bell containing Ar-saturated atmosphere for 3 min [68,69]. Flame-annealing (or sputter cleaning) is crucial for benchmarking polycrystalline Pt, in order to obtain a clean, well-defined and reproducible Pt surface. After flame-annealing, the electrode was cooled in an Ar. Once at room temperature, the electrode surface was protected with a droplet of H_2-saturated Millipore water, in order to mount the sample without introducing any sources of contamination from the atmosphere. The polycrystalline Pt sample was then mounted on the rotating disk electrode tip, using a previously sonicated polypropylene film as mounting stage [67]. Any residual hydrogenated water was carefully removed from the walls of the polycrystalline electrode using lens paper. Then, the RDE tip was inserted into the electrolyte under potential control (0.05 V *vs.* RHE). In this potential range, it is assumed that only H adsorption occurs and there is no oxidation of the surface [8,70]. We check the cleanliness of the system, and confirm that the flame-annealing and cooling procedures has been carried out correctly, by examining the features on the base cyclic voltammograms on polycrystalline Pt in N_2-saturated electrolyte, as we describe below. The ORR activity measured on flame-annealed polycrystalline Pt at 0.9 V *vs.* RHE using 1600 rpm and 50 mV/s scan rate is 1.9 ± 0.2 mA/cm^2 [70].

The same mounting procedure (except the flame-annealing) was were repeated for thin films. The potential was held at 0.05 V *vs*. RHE during immersion. Having potential control is crucial for thin films since potential spikes can cause damages to the sample surfaces and ultimately delamination. The sample was cycled between 0.05 and 1.00 V *vs.* RHE at 200 mV/s in N_2-saturated electrolyte for 200-300 cycles, rotating at 400 rpm. The exact number of cycles depends on the specific sample, since some thin films can have a bit rougher surfaces than others, or have been in contact with air longer and thus will require more cycling to obtain a stable CV.

The uncompensated Ohmic resistance in an electrochemical system derives from a sum of different resistance factors in the electrochemical circuit. In this case, it is dominated by the resistance of the electrolyte solution between the working electrode and the tip of the Luggin capillary [71]. This resistance also depends on external factors such as temperature, current density and pH. Therefore it

has to be evaluated for each measurement, in order to meaningfully compare the different samples. The Ohmic resistance was measured by means of electrochemical impedance spectroscopy (EIS) [71]. This method consists of measuring a *Nyquist* plot of the impedance. The real part of the impedance at high frequencies is largely due to the series resistance of the system, whereas the imaginary part of the impedance spectra relates to charge transfer and capacitive effects. The built-in series resistance is evaluated from the intersection of the linear regression of the imaginary impedance to the axis of the real impedance, typical evaluated in the 400 to 60 Hz range where noise contributions are negligible. No rotation was applied to the working electrode during this measurement, and the electrolyte was N_2-saturated. The measured Ohmic resistance *R* typically ranges from 25 to 30 Ω. The *IR* compensation was subsequently taken into account during the data treatment.

The RHE potential has been measured experimentally by bubbling H_2 while rotating the working electrode at 1600 rpm and cycling between -0.74 and -0.70 V *vs.* $Hg_{(l)}|HgSO_{4(g)}$. The value of the RHE potential can be read as the intercept with the current axes as this value represent the reduction/oxidation potential for hydrogen *i.e.* the RHE zero. Typical values for RHE potentials are between -0.717 and -0.725 V *vs.* $Hg_{(l)}|HgSO_{4(g)}$. Using the EIS and RHE technique explained, all data were thus corrected [70]:

$$U_{\mathrm{RHE}} = U_{\mathrm{Hg|HgSO_4}} - \Delta U_{\mathrm{Hg|HgSO_4-RHE}} - IR \qquad (2)$$

The ORR activity has been measured in O_2-saturated 0.1 M $HClO_4$ while cycling the working electrode between 0.00 and 1.00 V *vs.* RHE and rotating at 1600 rpm. The scan rate used was 50 mV/s and the sample was cycled until a stable CV was reached (normally around 20 cycles). It is important to note that a variety of scan rates have been used in the literature for measuring the ORR, which makes it challenging to directly compare results from different laboratories [70,72]. The ORR activity increases with increased scan rate, and it is unclear if this is due to some reconstruction of the surface or impurities [27]. At low scan rates, however, the CVs in N_2 and O_2 are not reproducible and they do not stabilize, therefore 50 mV/s has been chosen for the measurements [70].

2.3. Evaluation of the electrochemically active surface area (ECSA)

To properly compare the ORR activity of the Pt-based thin films, it is necessary to evaluate the electrochemically active surface area (ECSA), which is the area involved in the electrocatalytic reaction. Two commonly used methods to determine the ECSA are underpotential deposition of

hydrogen (H_{UPD}) and CO-stripping. Both methods rely on the adsorption of different species on the active site of the catalyst, and subsequently a total desorption of these species from the surface by applying an appropriate potential [72,73]. This "release" of charge can be evaluated by integrating over the relevant onset/offset potential and dividing by the scan rate as:

$$Q_{ECSA} = \frac{\mathrm{d}t}{\mathrm{d}U}\int_{U_{onset}}^{U_{offset}} I - I_{off}\,\mathrm{d}U \qquad (3)$$

Where d*U*/d*t* is the scan rate, $U_{onset/offset}$ relevant potential limits for the adsorption/desorption mechanism investigated and I_{off} is the background contribution of the CV. By evaluating the Q_{ECSA} one may estimate the ECSA area A_{ECSA} by assuming a pure Pt overlayer forms on the catalyst, and compare it to the charge per area estimates evaluated from extended Pt polycrystalline samples:

$$\frac{Q_{ECSA}^{ref.}}{A_{ECSA}^{ref.}} = \sigma_{\mathrm{Pt_{Poly}}}^{ref.} \Rightarrow A_{ECSA}^{ref.} = \frac{Q_{ECSA}^{ref.}}{\sigma_{\mathrm{Pt_{Poly}}}^{ref.}} \qquad (4)$$

Where the charge per area $\sigma_{Pt_{Poly}}^{ref.}$ is some relevant reference experimental value, in our case either the charge associated with H_{UPD} or that of CO oxidation on polycrystalline Pt.

2.3.1. Hydrogen underpotential deposition (H_{UPD})

This method consists of studying the affinity of the Pt electrode surface to adsorbed hydrogen by integrating the region corresponding to reversible underpotential deposited hydrogen, *i.e*. hydrogen adsorbing/desorbing at potentials more positive than the equilibrium potential for the hydrogen evolution reaction[10,72]. The H_{UPD} charges were compared to that of flame-annealed polycrystalline Pt, where the H_{UPD} charge area was $\sigma_{\mathrm{Pt_{Poly}}}^{\mathrm{H_{UPD}}} = 191 \pm 8$ μC/cm^2, based on 20 independent measurements. This value is consistent with other reports in the literature [10,74].

2.3.2. Stripping of carbon monoxide

The CO-stripping involves the electrochemical adsorption and oxidation of CO on Pt electrode surfaces, and the measurement of its potentiodynamic oxidation charge [75,76]. Similar to the H_{UPD}, the CO-stripping charge is correlated to that of polycrystalline Pt. The experimental procedure can be summarized as follows: The sample was cycled 3 times in Ar-saturated electrolyte at 10 mV/s. Then, the electrode was maintained at 0.05 V *vs.* RHE while bubbling CO for 3 min saturating the electrode surface. The electrode potential was maintained at 0.05 V *vs.* RHE for 30 min while bubbling Ar gas

purging the remaining CO from the electrolyte. The potential was then swept between 0.05 V and 1.00 V *vs.* RHE at 10 mV/s. The following anodic sweep exhibits the well-known CO oxidation peak of the CO adsorbed on the Pt surface, as:

$$CO + H_2O \rightarrow CO_2 + 2H^+ + 2e^- \quad (6)$$

Following the CO oxidation, the sample was cycled for a couple of scans ensuring no CO induced changes to the base CV and complete CO desaturation of the electrolyte occurred.

2.4. Stability measurements

We performed accelerated degradation tests on the thin films. These consisted of 10,000 potential cycles between 0.60 and 1.00 V *vs.* RHE in O_2-saturated electrolyte at 100 mV/s and room temperature (23 °C). The choice is based on the protocols of both the U.S. Department of Energy [77] and the Fuel Cell Commercialization Conference in Japan [78]. We note that further degradation may take place at elevated temperatures [79]. Following the stability test, we changed the electrolyte and measured the Ohmic resistance, RHE potential, and ORR activity. We must note that we changed the electrolyte under potential control and with great care towards the electrode integrity.

2.5. X-ray Photoemission Spectroscopy (XPS) and X-Ray Diffraction (XRD) measurements

X-Ray Diffraction (XRD) measurements have been performed with a PANalytical XPert Pro equipment with an X-ray wavelength of 0.154 nm for the $Cu_{K\alpha}$ line. The glancing incident X-ray diffraction spectroscopy (GI-XRD) was performed for angles from 20 ° to 90 °.

X-ray Photoemission Spectroscopy (XPS) spectra for Pt alloys were recorded using an instrument from Theta Probe (Thermo Scientific). The base pressure in the chamber was $5x10^{-10}$ mbar, the analysis was done with monochromatized $Al_{K\alpha}$ X-rays (1486.7 eV) and the electron energy analyzer had an acceptance angle of 60 °. No tilting of the sample was applied during measurement. Some samples were sputter cleaned to remove the first few layers of oxides and adsorbates from ambient sample transfer from deposition- to XPS chamber. This was done using a 0.5 keV Ar^+ 1.0 μA beam over a 6 x 6 mm^2 area for a few minutes. Several measurements on different locations of the samples were taken, using an X-ray beam spot size of 400 μm.

3. Results and discussion

3.1. Physical characterization

The XRD profile of a Pt thin film in comparison with the Pt powder reference is shown in Figure 3. It is possible to notice how the peaks match, meaning that a bulk structure of crystalline Pt is formed. The broadened peak around 43 ° is due to the interference from the carbon support. Figure 4 shows the XRD profile of a Pt_5Gd thin film, as compared with polycrystalline Pt_5Gd. The samples present a crystal structure similar to polycrystalline Pt_5Gd [46], and in accordance with the literature [80], with a hexagonal Cu_5Ca-type structure. This is an indication of the formation of an ordered intermetallic compound, even at the relatively low (300 °C) deposition temperature.

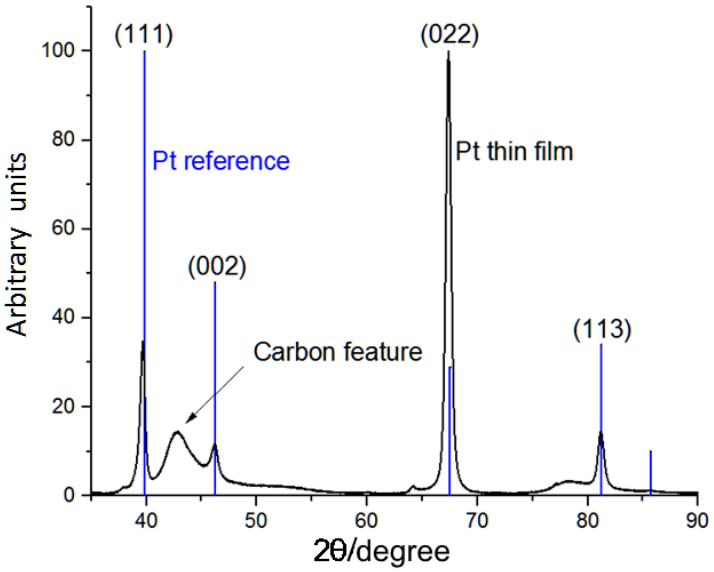

Figure 3. XRD on 40 nm Pt thin film deposited at 300 °C (black) as compared to Pt powder reference (blue).

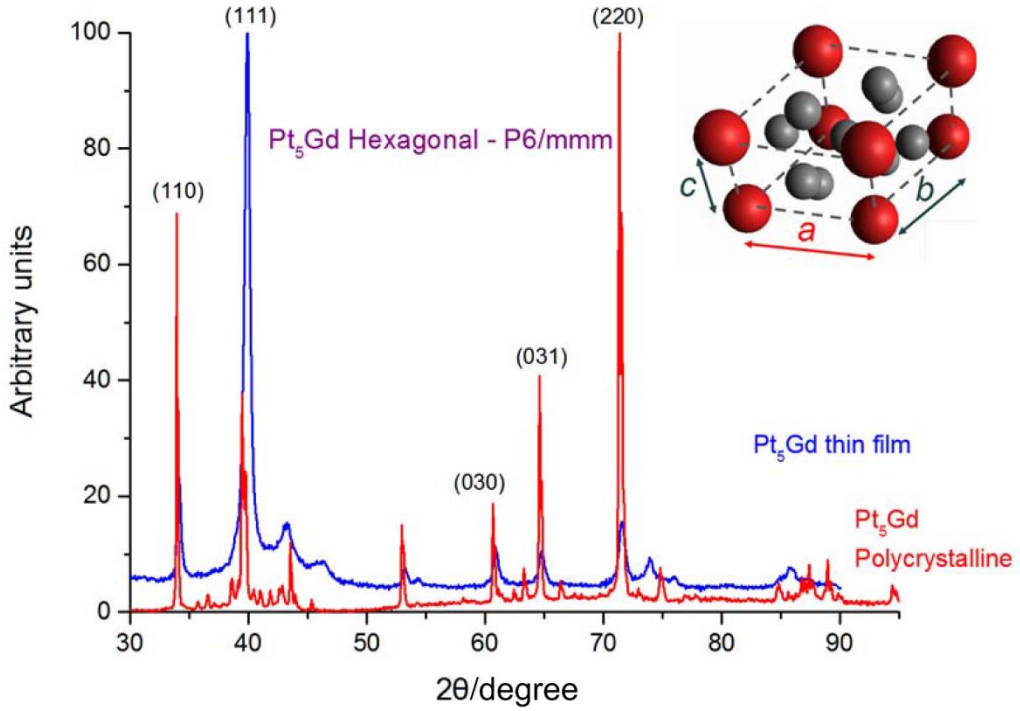

Figure 4. XRD on a 50 nm Pt_5Gd thin film deposited at 300 °C (blue) compared to Pt_5Gd polycrystalline (red), with a schematic of the obtained crystal structure.

Figure 5 shows the Pt4f and the Gd4d peaks of a Pt_5Gd thin film, as compared with bulk polycrystalline Pt_5Gd samples. The peaks have been plotted with background subtraction (*Shirley*-type) and matched with the same peaks of a polycrystalline Pt_5Gd reference sample. To ensure minimum signal from advantageous adsorbates after ambient transfer the samples were subjected to Ar sputter cleaning. Peak positions of the thin film seems to match those found for Pt_5Gd bulk sample, indicating a Pt-Gd containing alloy was formed [46]. However, from Figure 5b a slight shift on the order of 0.5 eV is observed for the Gd4d peak. This slight, but significant shift indicates at least some Gd-O coordination in the thin film surface and is caused by the fact that the thin films cannot be subjected to the same extended cleaning procedure as the polycrystalline sample due to their limited thickness.

To investigate the as-prepared thin film sample before and after electrochemical stability tests, XPS was conducted on samples which were not sputter cleaned. The *ex situ* XPS data obtained was moreover used as an indicator of unexpected species in the sputter deposited thin films. From the XPS survey (see Figure 6) and the zoom-ins of Pt4f, Gd4d, C1s and O1s peaks obtained before and after stability test (see Figure 5) we can deduce that no unexpected metallic components have been

incorporated into the thin films during fabrication. XPS zoom-ins of Pt4f, Gd4d, C1s and O1s peaks were also used to co-establish metallic ratios of the thin films. However, as XPS is a very surface sensitive technique and the as-prepared thin films are expected to energetically favor Pt surface termination, XPS could overestimate the metallic ratio of Pt *vs.* Gd.

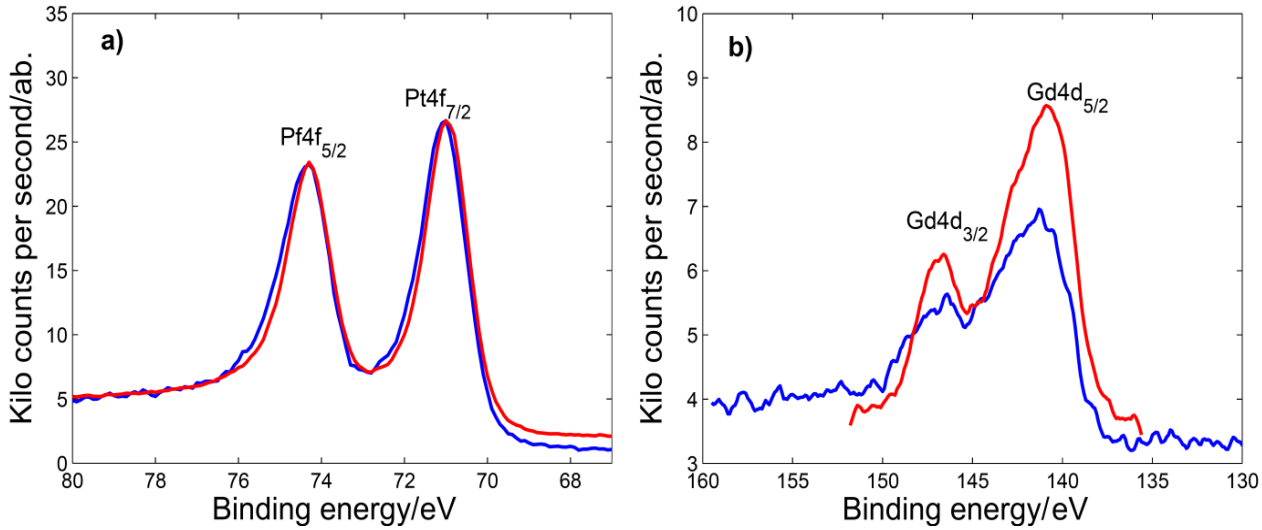

Figure 5. XPS spectra of (a) Pt4f peaks and (b) Gd4d peaks measured on a 50 nm Pt_5Gd thin film deposited at 300 °C (blue) and a bulk Pt_5Gd polycrystalline sample (red), both Ar sputter cleaned.

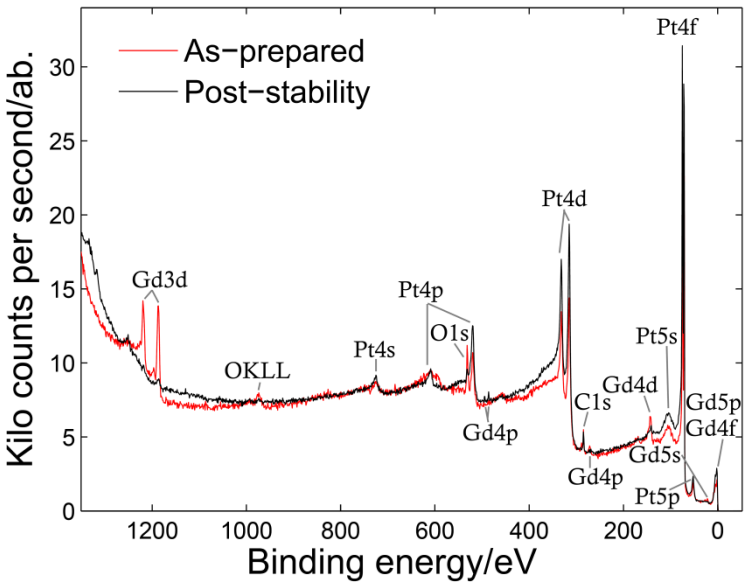

Figure 6. XPS survey of Pt_5Gd thin films as-prepared (red) and post 10,000 stability cycled (black), all samples subject to ambient conditions and not Ar sputter cleaned.

Figure 7 shows the non-sputter cleaned thin film sample as-prepared and after electrochemical tests (in both cases, the thin films had been ambient conditions before carrying out the XPS measurements). We were able to establish a rough elemental composition of the as-prepared films. The Pt:Gd:C:O composition percentages are respectively 40.0, 8.4, 28.6, and 23.0 %. The as-prepared Pt:Gd ratio from XPS is thus found to be 0.83:0.17, which corresponds to a 4.9 to 1.0 Pt:Gd ratio, close to the stoichiometric 5:1 ratio. Similarly, the Pt:Gd:C:O percentages of the Pt_5Gd thin films after stability test are respectively 68.5, 2.6, 25.0, and 3.9 %. In this case, the Pt to Gd ratio increased to 26.3 to 1.0, likely due to the formation of the thick Pt overlayer, in agreement with our previous observations on polycrystalline Pt-lanthanide alloys [8,46,48].

The peak associated with carbon in an oxidized state, denoted A in Figure 7a, disappear after electrochemistry, indicating that the carbon oxide has been removed from the surface of the thin film after the acid treatment. Moreover, Figure b indicates that at least some oxygen in a peak denoted B, likely in a metal-oxide state, is leached out the thin film in acid. One may speculate that the top-most layer of the as-prepared thin film consists of Pt, Gd, C, O and something resembling a native gadolinium oxide layer, which is removed during electrochemical cycling *i.e.* the surface of the thin film is somewhat oxidized however the bulk of the film is not.

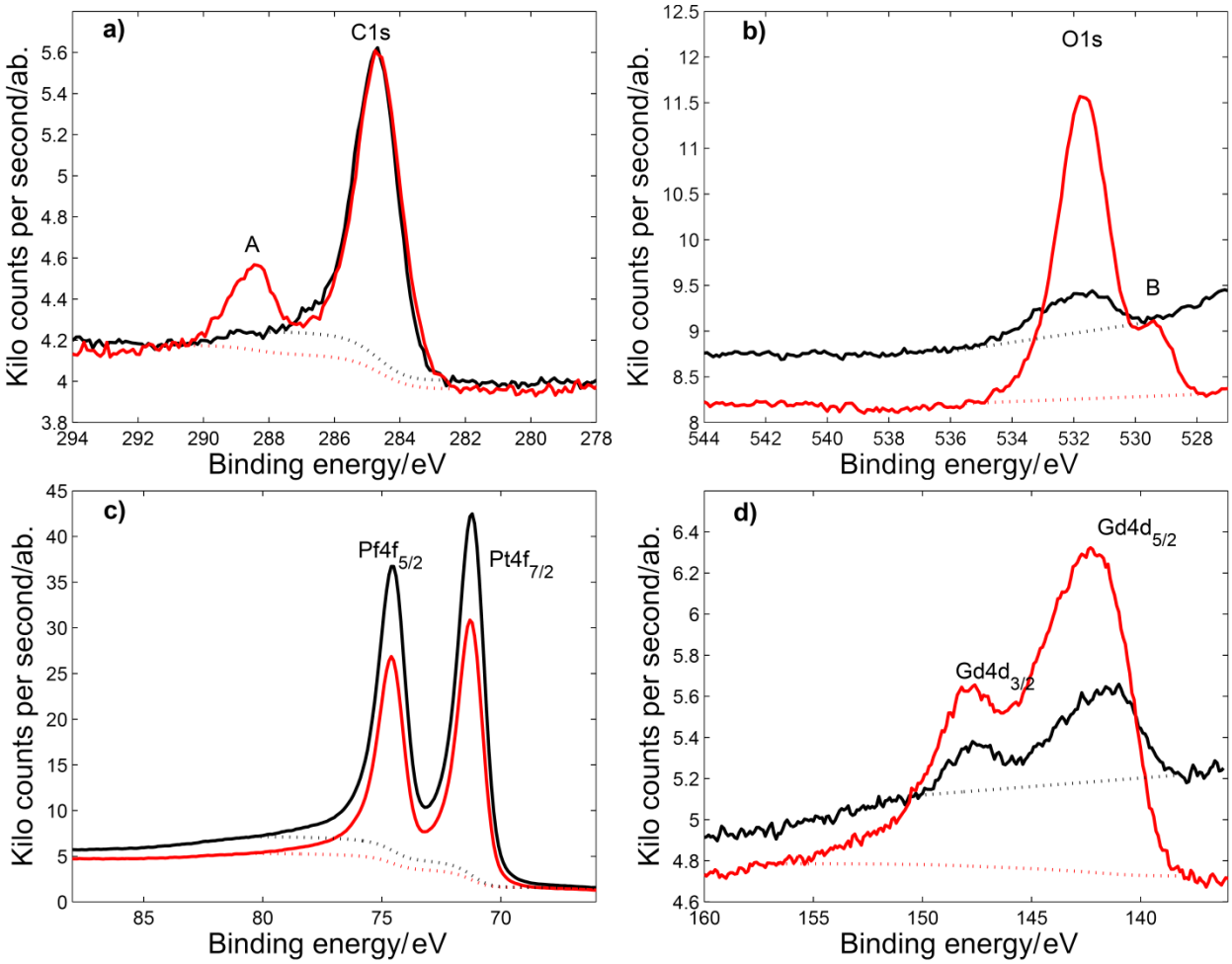

Figure 7. XPS survey zoom-ins of Pt_5Gd as-prepared (red) and post 10,000 stability cycled (black) thin films **(a)** C1s **(b)** O1s **(c)** Pt4f and **(d)** Gd4d peaks with Shirley background (dashed), all samples subject to ambient conditions and not Ar sputter cleaned.

3.2. Electrochemical characterization

3.2.1. Electrochemically active surface area

Figure 8 shows a CV of a Pt_5Gd thin film in N_2-staurated 0.1 M $HClO_4$. The H_{UPD} charge $Q_{ECSA}^{\mathrm{H_{UPD}}}$ can be obtained as the average of both the H adsorption and H desorption regions, as follows:

$$Q_{ECSA}^{\mathrm{H_{UPD}}} = \frac{\mathrm{d}t}{2\mathrm{d}U}\left[\int_{0.05\ \mathrm{V}\ vs.\ \mathrm{RHE}}^{\mathrm{H}_{ad.\ onset}} I - I(U_{\mathrm{H}_{ad.\ onset}})\,\mathrm{d}U + \int_{\mathrm{H}_{ad.\ offset}}^{0.05\ \mathrm{V}\ vs.\ \mathrm{RHE}} I - I(U_{\mathrm{H}_{ad.\ offset}})\,\mathrm{d}U\right] \quad (5)$$

The above H_{UPD} areas can be seen as the charge (blue) areas of Figure 8. For the Pt_5Gd thin film sample, the measured charge was $Q^{H_{UPD}}_{Pt_5Gd_{Thin\ film}} = 48.61\ \mu C$. If we divide this value by the charge density (4) of a polycrystalline surface, we can get an estimate of the surface area of the thin film sample**.** The lower limit of 0.05 V *vs.* RHE in (5) has been established empirically as it is unclear when the Pt surface goes from H adsorption to H_2 evolution [10,72]. We must note that the H_{UPD} region might also contain a contribution from anion adsorption at steps [81]. Moreover, hydrogen binding will vary from a flat polycrystalline sample compared to a rough one due to the increased presence of steps and kinks, locally changing the hydrogen saturation coverage [81].

Pt-based single-crystalline electrodes have been widely used as model surfaces to investigate the adsorption of H and OH [25,82]. The H_{UPD} area evaluation is also a commonly used technique for large surface Pt areas [72]. However, discrepancies may arise from alloying, since altering the electronic properties of the Pt surface may modify the binding of H [83]. As a consequence, the adsorption of H can be strongly suppressed by both strain and ligand effects, as recent works on both Pt-based single-crystalline [25,82–84] and polycrystalline [8] alloys demonstrate.

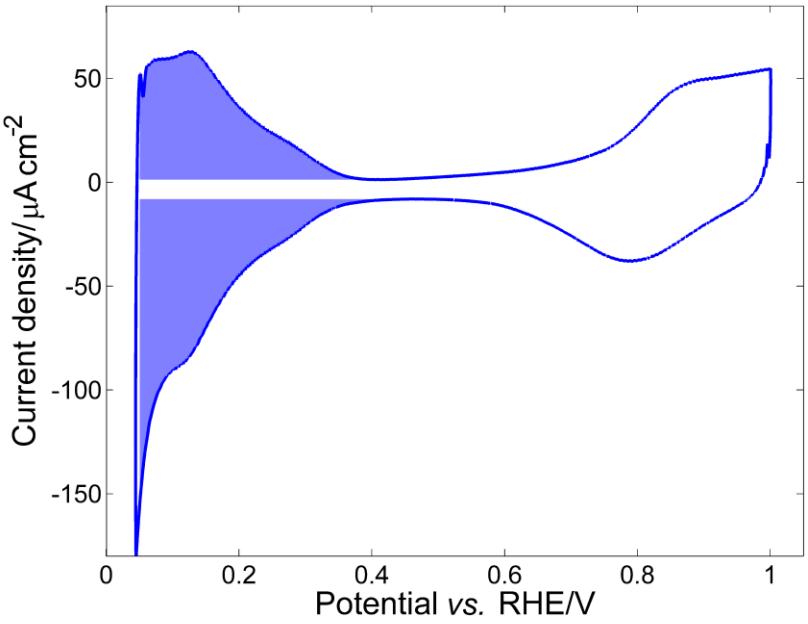

Figure 8. Base CV of a Pt_5Gd thin film with current densities evaluated using the geometric area of the electrode. The blue areas designate the charge area considered for ECSA evaluation using H_{UPD}. The CV is measured at room temperature, 50 mV/s and 400 rpm in N_2-saturated 0.1 M $HClO_4$.

The ECSA was also evaluated by the CO-stripping method. Figure 9 shows the characteristic CO oxidation peak of a Pt_5Gd thin film sample. If we subtract the anodic background from the CO-stripping cycle and integrate the CO oxidation peak between the two current intersects (from U_1 to U_2 in Figure 9), it is possible to estimate the CO charge:

$$Q_{ECSA}^{\mathrm{CO}} = \frac{\mathrm{d}t}{\mathrm{d}U}\int_{U_2}^{U_1} I - I_{background}\,\mathrm{d}U \qquad (7)$$

From the integral under the stripping peak, corrected against the background, we can evaluate the ECSA following (3).

The CO-stripping method is useful not only for the evaluation of the surface area, but also for gathering some insight into the surface morphology of the catalysts, as shifts in potential for CO desorption peak(s) gives information of the uniformity of the samples [76,85]. Varying CO desorption potentials may indicate different desorption sites available on the surface *e.g.* terrace, step, kink or edge sites [83,86,87]. As CO oxidation is likely a two electron transfer process (6), the CO-stripping charge area is approximately double that of H_{UPD}, therefore a value of 420 μC/cm^2 has previously been used in other studies [72,73]. However, from the evaluations on polycrystalline Pt samples, an empirical factor of 349 ± 9 μC/cm^2 was found from earlier studies [70,88]. Hence, for consitency, we used this factor for our thin films' ECSA evaluation. Although the CO-stripping method has been widely used for ECSA evaluation, we are aware that it can cause the rearrangement of the surface due to the strong CO binding to the Pt surface [73]. For instance, CO smoothens Pt(111) single-crystalline surfaces [67,87] but it can roughen Pt/C nanoparticles [89]. One benefit of the CO-stripping method as compared to the H_{UPD} area evaluation method is that the former is less sensitive to changes in adsorption/desorption potentials [83]. However, it is noteworthy to mention that changes in CO desorption potential (*e.g.* from varying the distribution of available step, terrace or kink sites) should shift the saturation coverages [83,90].

In the evaluation of the area using both the H_{UPD} and CO-stripping methods, we have assumed that, for the thin film samples, saturation coverages per area will match those of polycrystalline Pt. Moreover, we assume that ligand effects from Gd alloying do not play an important role in the H_{UPD} and CO adsorption/desorption potentials, due to the formation of a thick Pt overlayer (4 to 6 atomic layers of Pt) [8,46].

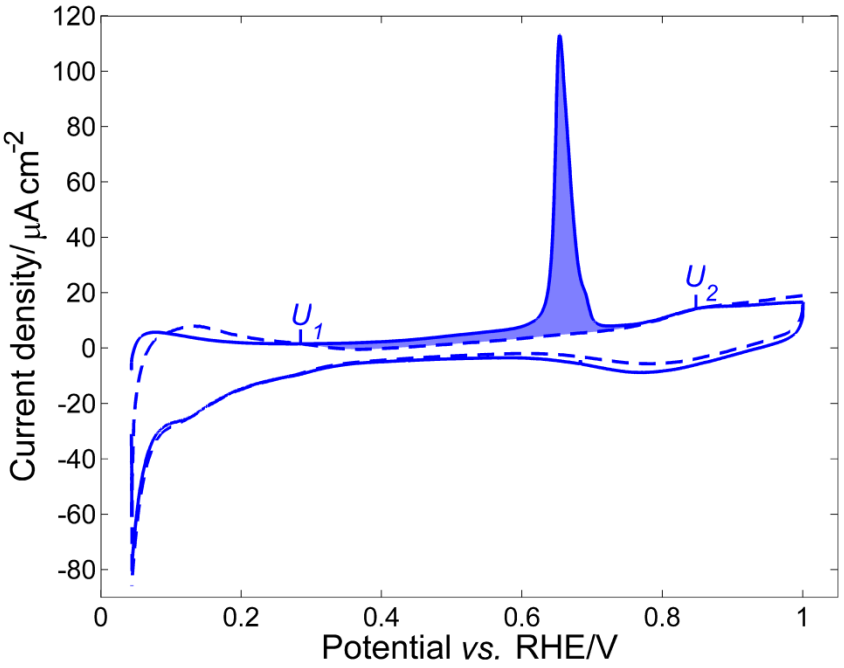

Figure 9. CO-stripping peak of a Pt_5Gd thin film sample. The blue area is the area considered for ECSA evaluation. Full line CV shows CO oxidation and dashed line the background cycle. In this case, a charge of $\boldsymbol{Q^{CO}_{Pt_5Gd_{Thin\ film}}} = \mathbf{81.15}\ \mu\mathbf{C}$ was found. The CV is measured at room temperature in $HClO_4$, at 10 mV/s with 200 rpm rotation during CO desorption and no rotation during the cycling.

In summary, we used CO-stripping evaluated ECSAs to normalize the specific activity of the Pt-based thin films. We chose the ECSA evaluated from the CO oxidation charge rather than the H_{UPD} region due to the fact that the H_{UPD} region is heavily affected by strain effects [82], as we observed both on polycrystalline Pt-lanthanide alloys [8] and Gd/Pt(111) single crystals [84]. Furthermore, the integration limits can be easily defined and it is possible to evaluate the Pt_5Gd thin film base CVs before and after CO-stripping, thus ensuring no significant changes in CV features arises from the CO-stripping procedure.

3.2.2. Cyclic voltammograms in the absence of oxygen

Figure 10 shows the evolution of the Pt_5Gd thin film surface when cycled in the N_2-saturated $HClO_4$ electrolyte. We observe that the shape or the CVs changes with cycling, especially during the first 50 cycles. This is partially due to the removal of surface impurities that had been deposited during transport between the sputter chamber and the electrochemical setup, but mostly due to the formation

of the Pt overlayer, and to the rearrangement of the surface to a minimum energy (stable) condition. Observing the rearrangement of the CVs is important since it is an indication of both the formation of the right catalysts surface and the cleanliness of the RDE setup apparatus. The initial activation cycles are performed at 50 mV/s in order to monitor and observe the evolution of the CVs. However, once a set behaviour of the evolution of the Pt_5Gd thin film samples have been established, one may prefer to perform accelerated activation cycling (*e.g.* at 200 mV/s), as this lowers overall experiment time, minimizing contamination issues from prolonged electrochemical exposure.

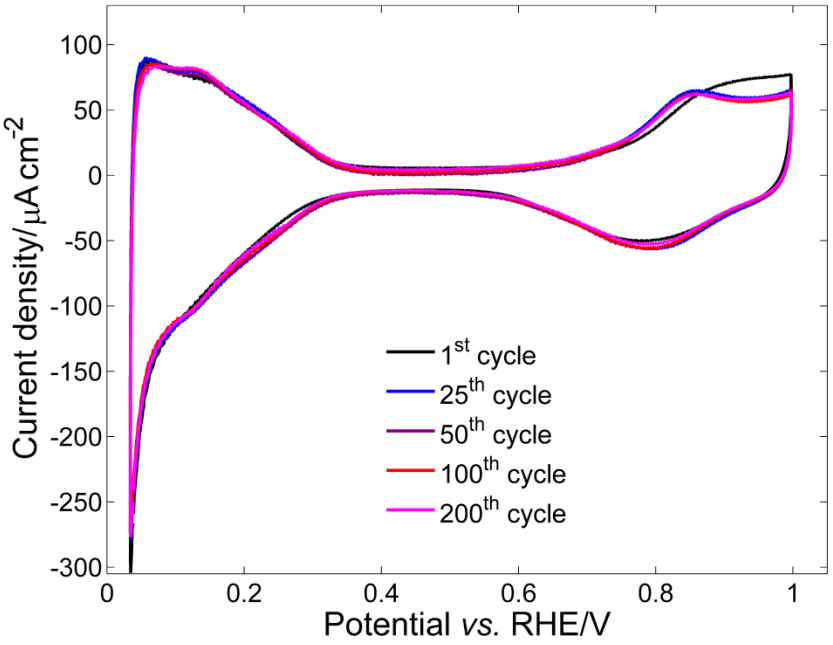

Figure 10. Activation CVs in N_2-saturated 0.1 M $HClO_4$ at room temperature, 50 mV/s and 400 rpm for a Pt_5Gd thin film.

Figure 11 shows the CVs in N_2-saturated electrolyte of a Pt thin film compared with a flame-annealed bulk polycrystalline Pt (Pt_{Poly}). The observed differences in the CVs indicate different surface structure for the two Pt samples. This results in distinct adsorption/desorption energies for H, OH and O [81]. Nevertheless, the roughness estimated with H_{UPD} method difference less than 10 % for the Pt and Pt_5Gd thin film samples (see Table 1). We note the difference in the distinctiveness of the features associated with hydrogen adsorption/desorption at Pt(110) step sites at ~0.12 V *vs*. RHE and at Pt(100) step sites at ~0.28 V *vs*. RHE [91]. It is observed that thin films have lower amount of (100) sites than polycrystalline Pt, which would be in agreement with an increase of (111) domains [92]. Moreover, it

is worth mentioning that the presence of the (110) and (100) features in the polycrystalline Pt CVs indicates good cleanliness of the system, and shows that the flame-annealing procedure have been appropriately conducted [93].

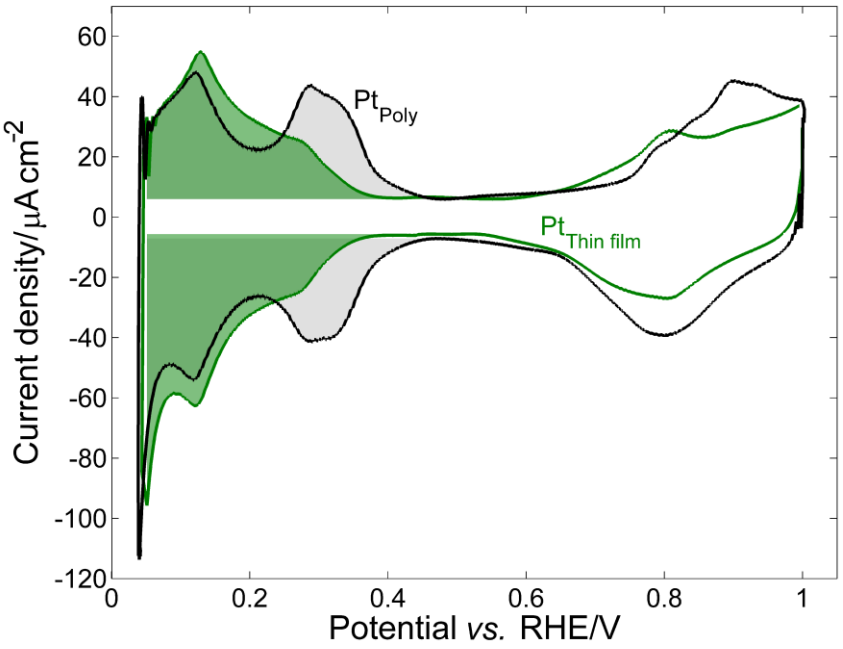

Figure 11. Base CVs in N_2-saturated 0.1 M $HClO_4$ electrolyte of a Pt thin film (30 nm) deposited at 300 °C (green) compared with polycrystalline Pt (black), measured at room temperature, 400 rpm and 50 mV/s scan rate.

Table 1. Roughness and ECSA for the different samples.

*For extended surfaces, ECSA has been defined as the geometric electrode area.

	Roughness Factor (H_{UPD})	**Roughness Factor (CO-stripping)**	$A_{ECSA}^{H_{UPD}}$ **in [cm²]**	A_{ECSA}^{CO} **in [cm²]**
Pt polycrystalline*	1.0	1.0	0.196	0.196
Pt_5Gd polycrystalline*	1.0	1.0	0.196	0.196
Pt thin films	0.9 ± 0.1	1.0 ± 0.1	0.18 ± 0.04	0.19 ± 0.04
Pt_5Gd thin films	1.6 ± 0.4	1.4 ± 0.2	0.25 ± 0.12	0.26 ± 0.08

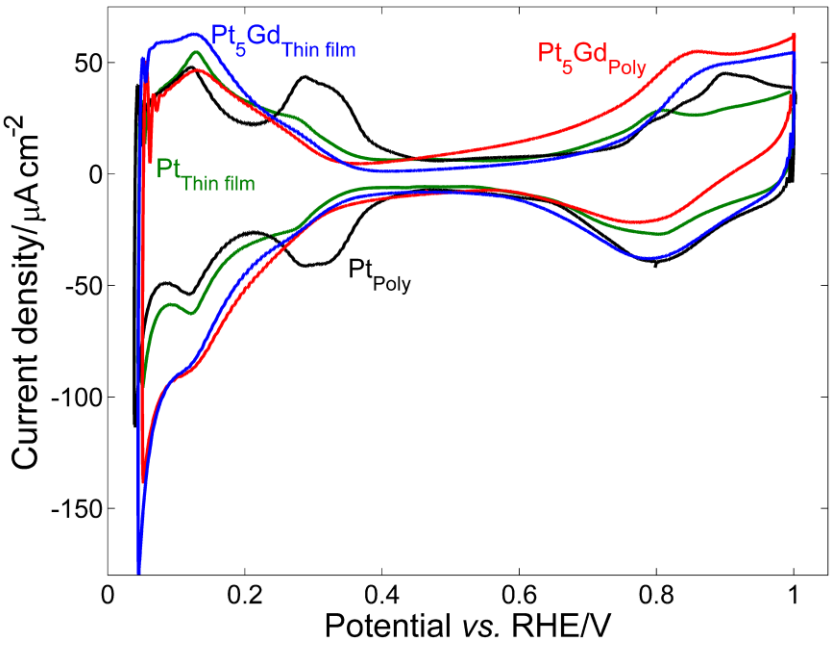

Figure 12. CVs of a Pt_5Gd thin film (50 nm thick) compared with polycrystalline Pt_5Gd, Pt thin film (15 nm thick) and polycrystalline Pt. All CVs are measured in N_2-saturated 0.1 M $HClO_4$ at room temperature, with a rotation speed of 400 rpm, at 50 mV/ s.

The CVs in N_2-saturated electrolyte of a Pt_5Gd thin film compared with Pt_5Gd polycrystalline sample and pure Pt are shown in Figure 12. As can be observed, the shape of the CVs on both Pt_5Gd thin film and polycrystalline Pt_5Gd presents similar characteristic features. The similar H adsorption region of the Pt_5Gd thin film and bulk crystalline sample suggests comparable surface areas. We estimated the roughness of the thin films using the CO-stripping method. Table 1 shows the roughness factors (calculated as the ratio A_{ECSA}/A_{geo}), and the average electrochemical surface area for the thin films as well as the polycrystalline samples. Figure shows the comparison between typical CO-stripping peaks for Pt and Pt_5Gd thin films. The roughness of the thin films is comparable with that of the polycrystalline samples, suggesting similar surface morphology, *i.e.* polycrystallinity [46]. We also show a typical CO-stripping CV on a bulk polycrystalline Pt electrode. The pre-peak on polycrystalline Pt can be explained by the stripping of CO adsorbed at step sites, as proposed by *Cuesta et al*. [93].

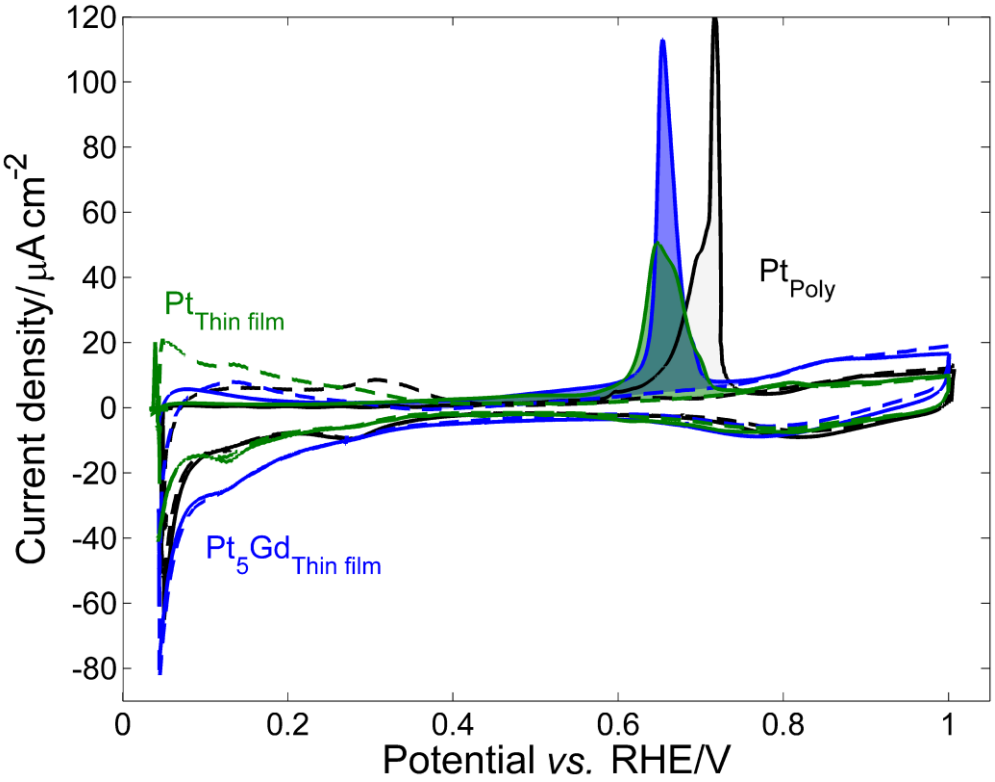

Figure 13. CO-stripping peaks for Pt and Pt_5Gd thin films compared with the CO-stripping on polycrystalline Pt. All the CVs were recorded in Ar-saturated 0.1 M $HClO_4$ at 10 mV/s and 200 rpm at room temperature. In this case, charges of $Q^{CO}_{Pt_5Gd_{Thin\ film}}$ = 81.14 μC (blue) and $Q^{CO}_{Pt_{Thin\ film}}$ = 67.32 μC (green) was found, corresponding to roughness factors of 1.2 and 1.0, respectively.

3.2.3. Oxygen reduction reaction activity and stability

The ORR catalytic activity was obtained in O_2-saturated electrolyte, cycling in a potential range between 0.00 and 1.00 V *vs.* RHE. Figure 14a shows the CVs on Pt and Pt_5Gd thin films, as well as polycrystalline Pt and Pt_5Gd, for comparison, in O_2-saturated 0.1 M $HClO_4$. Evidently, there is a considerable positive shift in the electrocatalytic activity of both Pt_5Gd thin films, as compared to pure Pt thin films and polycrystalline Pt, in the potential region of mixed kinetic transport. This means that the overpotential for the Pt_5Gd thin films has been substantially decreased, similar to our previous results on sputter-cleaned polycrystalline Pt_5Gd [8,46]. Mass-transport corrected kinetic current j_k can be extrapolated from the *Koutecky-Levich* relation [94]:

$$\frac{1}{j} = \frac{1}{j_k} + \frac{1}{j_l} \qquad (8)$$

Where j is the measured total current density (corrected with the A_{ECSA}) and j_l is the measured diffusion limited current density.

To have a graphic comparison of the catalytic activities, the logarithm of the kinetic current is plotted against the RHE potential to obtain a *Tafel* plot. Figure 14b shows the Tafel plots for Pt_5Gd thin film, polycrystalline Pt_5Gd, Pt thin film and polycrystalline Pt. The specific activities, *i.e.* the kinetic current density values, are calculated at 0.9 V *vs.* RHE. Pt_5Gd thin films show a 4.5-fold improvement in specific ORR activity compared to polycrystalline Pt, with an activity of 9.0 ± 0.6 mA/cm^2, and the result is comparable with the one obtained for polycrystalline Pt_5Gd exhibiting specific activities of 10.6 ± 0.5 mA/cm^2 [8]. Figure 14 also shows that the ORR activity of Pt thin films is considerably larger than that of bulk polycrystalline Pt. This is consistent with the (110)-like voltammetric features in the in the base CVs (Figures 11 and 12), as (110) steps [12,13,95] seem to enhance the ORR activity.

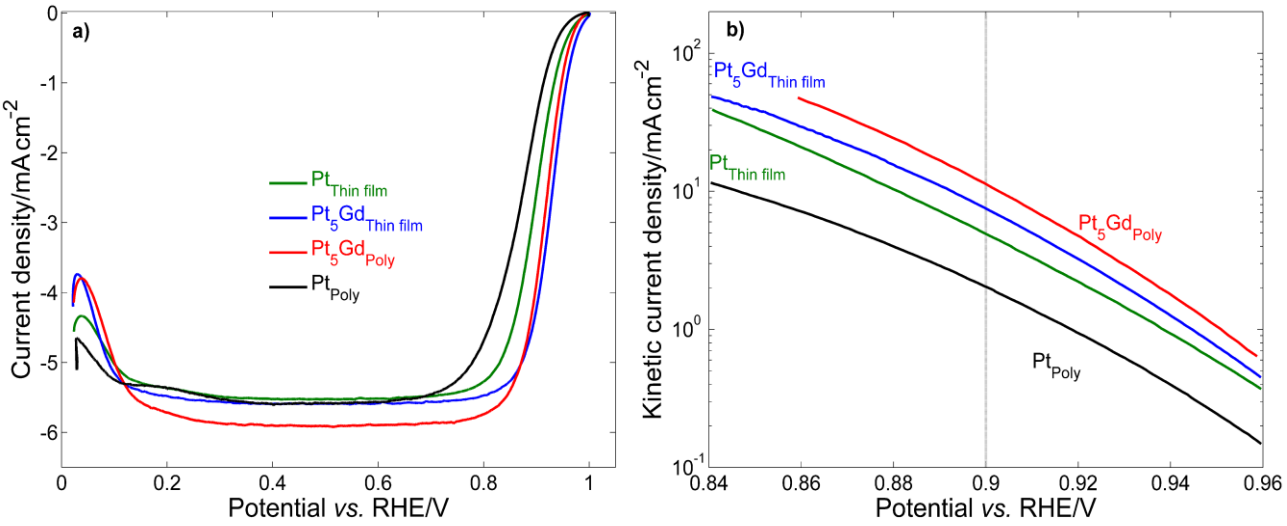

Figure 14. ORR activity plots of Pt_5Gd and Pt thin films and polycrystalline samples, all obtained in O_2-saturated 0.1 M $HClO_4$ at room temperature, 50 mV/s scan rate and 1600 rpm. **(a)** Anodic sweep of the geometric current density. **(b)** Tafel plot showing the kinetic current density evaluated using the CO evaluated ECSA.

ORR stability is also of profound relevance for ORR catalysts [6,8]. We carried out stability tests consisting of 10,000 cycles between 0.60 and 1.00 V *vs.* RHE in O_2-saturated $HClO_4$. Figure 15 shows the activity and stability of Pt_5Gd 50 nm thin films as compared with polycrystalline Pt_5Gd. The activities for both Pt thin films and polycrystalline Pt have also been plotted for comparison. Overall,

the thin films maintained around 80% of their initial activities, which is a value comparable to the one obtained for polycrystalline samples (around 85%). This means that the overall Pt_5Gd thin films activity is almost 5 times higher than the one of polycrystalline Pt and more than doubles the one for pure Pt thin films, while still showing a >3-fold improvement over polycrystalline Pt after stability test.

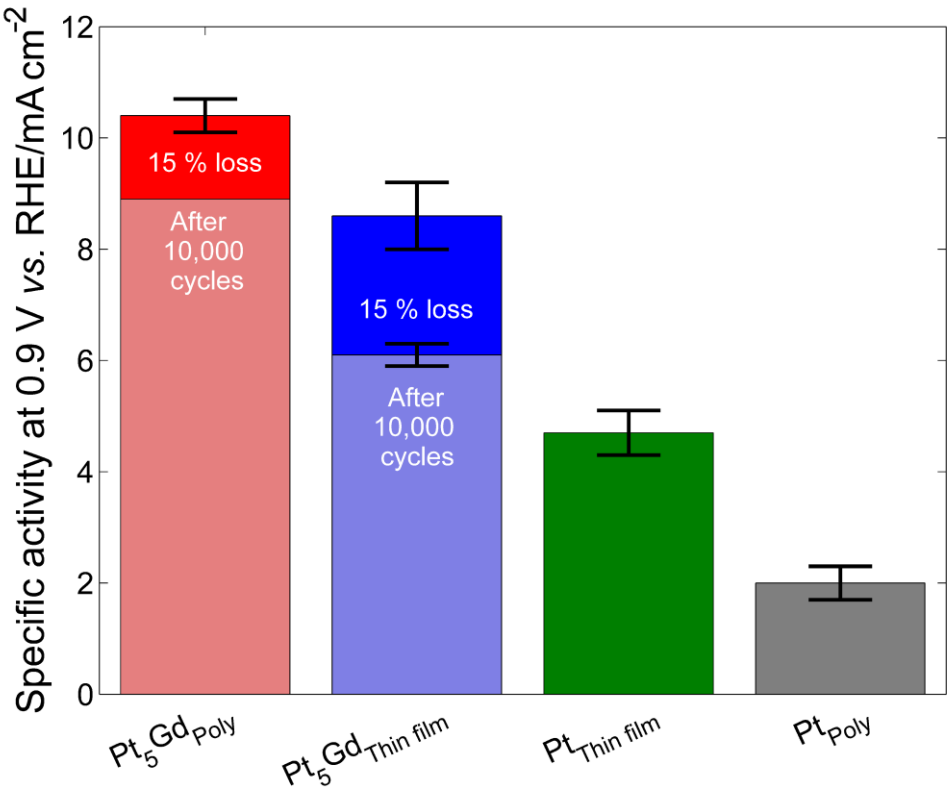

Figure 15. Specific activity at 0.9 V *vs.* RHE of Pt_5Gd thin films and polycrystalline samples before and after stability tests, compared with pure Pt thin film and polycrystalline samples.

4. Conclusions

In this study, we present the fabrication of Pt_5Gd thin films *via* sputter deposition under UHV conditions, underlying the importance of an oxygen-free environment when dealing with lanthanides. We show benchmarking protocols to test the electrochemical performance of Pt-lanthanide thin films by means of cyclic voltammetry. XPS and XRD show the successful formation of an oxygen-free Pt_5Gd thin film alloy, with a hexagonal Cu_5Ca-type structure, in agreement with previous reports on polycrystalline Pt_5Gd [8,46]. We have used the rotating ring disk electrode technique to measure the

ORR activities in acidic environment. Pt_5Gd thin films show a 4.5-fold improvement compared to pure polycrystalline Pt, and a 2.5-fold improvement compared to Pt thin films. Pt_5Gd presented similar stability than polycrystalline Pt_5Gd [46], retaining *ca.* 80% of their initial ORR activity. The presented methods will facilitate the future fabrication and characterization of thin films and investigation of Pt-lanthanides alloys, enabling an easy comparison between different ORR catalysts. It also paves the way for thin films catalysts of Pt-rare earth alloys to be implemented and tested as ORR catalysts in PEMFCs.

Acknowledgments

We gratefully acknowledge the Danish Council for Strategic Research's project NACORR (12-133817) for funding this work. This work was supported by a research grant (9455) from VILLUM FONDEN. M.E.-E. acknowledges the Danish Council for Independent Research for her Individual Postdoctoral grant and Sapere Aude: Research Talent grant. K. D. J. acknowledges funding from the KDFuelCell project of Denmark's Innovation Fund, project 20735.

References

[1] M.K. Debe, Electrocatalyst approaches and challenges for automotive fuel cells, Nature. 486 (2012) 43–51. doi:10.1038/nature11115.

[2] A. Rabis, P. Rodriguez, T.J. Schmidt, Electrocatalysis for Polymer Electrolyte Fuel Cells : Recent Achievements and Future Challenges, ACS Catal. 2 (2012) 864–890. doi:10.1021/cs3000864.

[3] F.T. Wagner, B. Lakshmanan, M.F. Mathias, Electrochemistry and the future of the automobile, J. Phys. Chem. Lett. 1 (2010) 2204–2219. doi:10.1021/jz100553m.

[4] Y. Nie, L. Li, Z. Wei, Recent advancements in Pt and Pt-free catalysts for oxygen reduction reaction., Chem. Soc. Rev. 44 (2015) 2168–201. doi:10.1039/c4cs00484a.

[5] S. Chu, Y. Cui, N. Liu, The path towards sustainable energy, Nat. Mater. 16 (2016) 16–22. doi:10.1038/nmat4834.

[6] A. Kongkanand, M.F. Mathias, The Priority and Challenge of High-Power Performance of Low-Platinum Proton-Exchange Membrane Fuel Cells, J. Phys. Chem. Lett. 7 (2016) 1127–1137. doi:10.1021/acs.jpclett.6b00216.

[7] I.E.L. Stephens, A.S. Bondarenko, U. Grønbjerg, J. Rossmeisl, I. Chorkendorff, Understanding the electrocatalysis of oxygen reduction on platinum and its alloys, Energy Environ. Sci. 5 (2012) 6744. doi:10.1039/c2ee03590a.

[8] M. Escudero-Escribano, P. Malacrida, M. H. Hansen, U. G. Vej-Hansen, A. Velázquez-Palenzuela, V. Tripkovic, J. Schiøtz, J. Rossmeisl, I. E. L. Stephens, Tuning the activity of Pt alloy electrocatalysts by means of the lanthanide contraction, Science. 352 (2016) 73–76. doi:10.1126/science.aad8892.

[9] V. Stamenkovic, B.S. Mun, K.J.J. Mayrhofer, P.N. Ross, N.M. Markovic, J. Rossmeisl, J. Greeley, J.K. Nørskov, Changing the activity of electrocatalysts for oxygen reduction by tuning the surface electronic structure, Angew. Chemie - Int. Ed. 45 (2006) 2897–2901. doi:10.1002/anie.200504386.

[10] P.N. Ross Jr., N.M. Markovic, Surface science studies of model fuel cell electrocatalysts, Surf. Sci. Rep. 45 (2002) 117–229.

[11] A.S. Bandarenka, H. a Hansen, J. Rossmeisl, I.E.L. Stephens, Elucidating the activity of stepped Pt single crystals for oxygen reduction., Phys. Chem. Chem. Phys. 16 (2014) 13625–13629. doi:10.1039/c4cp00260a.

[12] A. Hitotsuyanagi, M. Nakamura, N. Hoshi, Structural effects on the activity for the oxygen reduction reaction on n(111)–(100) series of Pt: correlation with the oxide film formation, Electrochim. Acta. 82 (2012) 512–516. doi:10.1016/j.electacta.2012.03.133.

[13] A. Kuzume, E. Herrero, J.M. Feliu, Oxygen reduction on stepped platinum surfaces in acidic media, J. Electroanal. Chem. 599 (2007) 333–343. doi:10.1016/j.jelechem.2006.05.006.

[14] R. Jinnouchi, K. Kodama, A. Nagoya, Y. Morimoto, Simulated Volcano Plot of Oxygen Reduction Reaction on Stepped Pt Surfaces, Electrochim. Acta. 230 (2017) 470–478. doi:10.1016/j.electacta.2017.02.034.

[15] F. Calle-Vallejo, J. Tymoczko, V. Colic, Q. Huy Vu, M. Pohl, K. Morgenstern, D. Loffreda, P. Sauteut, W. Schuhmann, A.S. Bandarenka, Finding optimal surface sites on heterogeneous catalysts by counting nearest neighbors, Science 350 (2015) 185–190.

[16] P.P. Lopes, D. Strmcnik, D. Tripkovic, J.G. Connell, V. Stamenkovic, N.M. Markovic, Relationships between Atomic Level Surface Structure and Stability/Activity of Platinum Surface Atoms in Aqueous Environments, ACS Catal. 6 (2016) 2536–2544. doi:10.1021/acscatal.5b02920.

[17] J.K. Nørskov, J. Rossmeisl, A. Logadottir, L. Lindqvist, D.- Lyngby, H. Jo, Origin of the Overpotential for Oxygen Reduction at a Fuel-Cell Cathode, Ournal Phys. Chem. B. 108 (2004) 17886–17892.

[18] S.M. Qingying Jia, Wentao Liang, Michael K. Bates, Prasanna Mani, Wendy Lee, Activity Descriptor Identi fi cation for Oxygen Reduction on Platinum-Based Bimetallic Nanoparticles : In Situ Observation of the Linear Relationship, Acsnano. 9 (2015) 387–400.

[19] S. Mukerjee, S. Srinivasan, P.M. Soriaga, J. McBreen, Role of Structural and Electronic Properties of Pt and Pt Alloys on Electrocatalysis of Oxygen Reduction. An insitu XANES and EXAFS investigation, J. Electrochem. Soc. 142 (1995) 1409. doi:10.1149/1.2048590.

[20] D. Strmcnik, M. Escudero-Escribano, K. Kodama, V.R. Stamenkovic, A. Cuesta, N.M. Marković, Enhanced electrocatalysis of the oxygen reduction reaction based on patterning of platinum surfaces with cyanide., Nat. Chem. 2 (2010) 880–885. doi:10.1038/nchem.771.

[21] V.R. Stamenkovic, B. Fowler, B.S. Mun, G. Wang, P.N. Ross, C.A. Lucas, N.M. Markovic, Improved oxygen reduction activity on Pt3Ni (111) via increased surface site availability, Science. 315 (2007) 493–

497. doi:10.1126/science.1135941.

[22] T. Toda, H. Igarashi, H. Uchida, M. Watanabe, Enhancement of the electroreduction of Oxygen on Pt alloys with Fe, Ni, and Co, J. Electrochem. Soc. 146 (1999) 3750–3756. doi:10.1149/1.1392544.

[23] P. Strasser, S. Koh, T. Anniyev, J. Greeley, K. More, C. Yu, Z. Liu, S. Kaya, D. Nordlund, H. Ogasawara, M.F. Toney, A. Nilsson, Lattice-strain control of the activity in dealloyed core–shell fuel cell catalysts, Nat. Chem. 2 (2010) 454–460. doi:10.1038/nchem.623.

[24] M. Mavrikakis, B. Hammer, J. Nørskov, Effect of Strain on the Reactivity of Metal Surfaces, Phys. Rev. Lett. 81 (1998) 2819–2822. doi:10.1103/PhysRevLett.81.2819.

[25] I.E.L. Stephens, A.S. Bondarenko, F.J. Perez-Alonso, F. Calle-Vallejo, L. Bech, T.P. Johansson, A.K. Jepsen, R. Frydendal, B.P. Knudsen, J. Rossmeisl, I. Chorkendorff, Tuning the activity of Pt(111) for oxygen electroreduction by subsurface alloying, J. Am. Chem. Soc. 133 (2011) 5485–5491. doi:10.1021/ja111690g.

[26] J.R. Kitchin, J.K. Nørskov, M.A. Barteau, J.G. Chen, Modification of the surface electronic and chemical properties of Pt(111) by subsurface 3d transition metals, J. Chem. Phys. 120 (2004) 10240–10246. doi:10.1063/1.1737365.

[27] H.A. Gasteiger, S.S. Kocha, B. Sompalli, F.T. Wagner, Activity benchmarks and requirements for Pt, Pt-alloy, and non-Pt oxygen reduction catalysts for PEMFCs, Appl. Catal. B Environ. 56 (2005) 9–35. doi:10.1016/j.apcatb.2004.06.021.

[28] V.R. Stamenkovic, B.S. Mun, M. Arenz, K.J.J. Mayrhofer, C. a Lucas, G.F. Wang, P.N. Ross, N.M. Markovic, Trends in electrocatalysis on extended and nanoscale Pt-bimetallic alloy surfaces, Nat. Mater. 6 (2007) 241–247. doi:10.1038/nmat1840.

[29] P. Mani, R. Srivastava, P. Strasser, Dealloyed binary PtM3 (M=Cu, Co, Ni) and ternary PtNi3M (M=Cu, Co, Fe, Cr) electrocatalysts for the oxygen reduction reaction: Performance in polymer electrolyte membrane fuel cells, J. Power Sources. 196 (2011) 666–673. doi:10.1016/j.jpowsour.2010.07.047.

[30] V.R. Stamenkovic, B.S. Mun, K.J.J. Mayrhofer, P.N. Ross, N.M. Markovic, Effect of Surface Composition on Electronic Structure , Stability , and Electrocatalytic Properties of Pt-Transition Metal Alloys : Pt-Skin versus Pt-Skeleton Surfaces, J. Am. Chem. Soc. 128 (2006) 8813–8819.

[31] D. Van Der Vliet, C. Wang, M. Debe, R. Atanasoski, N.M. Markovic, V.R. Stamenkovic, Platinum-alloy nanostructured thin film catalysts for the oxygen reduction reaction, Electrochim. Acta. 56 (2011) 8695–8699. doi:10.1016/j.electacta.2011.07.063.

[32] M.N. Markovic, T.J. Schmidt, V. Stamenkovic, P.N. Ross , 1 (2001) 105-116. doi:10.1002/1615-6854(200107)1:2<105::AID-FUCE105>3.0.CO;2-9.

[33] L. Wan, T. Moriyama, M. Ito, M. Watanabe, In situ STM imaging of surface dissolution and rearrangement of a Pt – Fe alloy electrocatalyst in electrolyte solution, (2002) 58–59. doi: 10.1039/B107037A.

[34] K.J.J. Mayrhofer, K. Hartl, V. Juhart, M. Arenz, Degradation of carbon-supported Pt bimetallic nanoparticles by surface segregation, J. Am. Chem. Soc. 131 (2009) 16348–16349. doi:10.1021/ja9074216.

[35] S. Mezzavilla, S. Cherevko, C. Baldizzone, E. Pizzutilo, G. Polymeros, K.J.J. Mayrhofer, Experimental Methodologies to Understand Degradation of Nanostructured Electrocatalysts for PEM Fuel Cells: Advances and Opportunities, ChemElectroChem. 3 (2016) 1524–1536. doi:10.1002/celc.201600170.

[36] B. Han, C.E. Carlton, A. Kongkanand, R.S. Kukreja, B.R. Theobald, L. Gan, R. O'Malley, P. Strasser, F.T. Wagner, Y. Shao-Horn, Record activity and stability of dealloyed bimetallic catalysts for proton exchange membrane fuel cells, Energy Environ. Sci. 8 (2015) 258–266. doi:10.1039/C4EE02144D.

[37] C. Chen, Y. Kang, Z. Huo, Z. Zhu, W. Huang, H.L. Xin, J.D. Snyder, D. Li, J.A. Herron, M. Mavrikakis, M. Chi, K.L. More, Y. Li, N.M. Markovic, G.A. Somorjai, P. Yang, V.R. Stamenkovic, Highly crystalline multimetallic nanoframes with three-dimensional electrocatalytic surfaces, Science. 343 (2014) 1339–1343. doi:10.1126/science.1249061.

[38] X. Huang, Z. Zhao, L. Cao, Y. Chen, E. Zhu, Z. Lin, M. Li, A. Yan, A. Zettl, Y.M. Wang, X. Duan, T. Mueller, Y. Huang, High-performance transition metal – doped Pt3Ni octahedra for oxygen reduction reaction, Science. 348 (2015) 1230–1234. doi:10.1126/science.aaa8765.

[39] L. Bu, N. Zhang, S. Guo, X. Zhang, J. Li, J. Yao, T. Wu, G. Lu, J.-Y. Ma, D. Su, X. Huang, Biaxially strained PtPb/Pt core/shell nanoplate boosts oxygen reduction catalysis, Science. 354 (2016) 1410–1414. doi:10.1126/science.aah6133.

[40] M. Li, M. Li, Z. Zhao, T. Cheng, A. Fortunelli, C. Chen, R. Yu, L. Gu, B. Merinov, Z. Lin, E. Zhu, T. Yu, Q. Jia, J. Guo, L. Zhang, W.A.G. Iii, Y. Huang, X. Duan, Ultrafine jagged platinum nanowires enable ultrahigh mass activity for the oxygen reduction reaction, Science. 354 (2016). doi:10.1126/science.aaf9050.

[41] L. Dubau, M. Lopez-Haro, L. Castanheira, J. Durst, M. Chatenet, P. Bayle-Guillemaud, L. Guétaz, N. Caqué, E. Rossinot, F. Maillard, Probing the structure, the composition and the ORR activity of Pt3Co/C nanocrystallites during a 3422 h PEMFC ageing test, Appl. Catal. B Environ. 142–143 (2013) 801–808.

[42] I.E.L. Stephens, J. Rossmeisl, I. Chorkendorff, Toward sustainable fuel cells, Science. 354 (2016) 1378–1379.

[43] I.E.L. Stephens, A.S. Bondarenko, L. Bech, I. Chorkendorff, Oxygen Electroreduction Activity and X-Ray Photoelectron Spectroscopy of Platinum and Early Transition Metal Alloys - Supporting information, ChemCatChem. 4 (2012) 341–349. doi:10.1002/cctc.201100343.

[44] J. Greeley, I.E.L. Stephens, a S. Bondarenko, T.P. Johansson, H. a Hansen, T.F. Jaramillo, J. Rossmeisl, I. Chorkendorff, J.K. Nørskov, Alloys of platinum and early transition metals as oxygen reduction electrocatalysts., Nat. Chem. 1 (2009) 552–556. doi:10.1038/nchem.367.

[45] T.P. Johansson, E.T. Ulrikkeholm, P. Hernandez-Fernandez, P. Malacrida, H. a. Hansen, a. S. Bandarenka, J.K. Nørskov, J. Rossmeisl, I.E.L. Stephens, I. Chorkendorff, Pt Skin Versus Pt Skeleton Structures of Pt3Sc as Electrocatalysts for Oxygen Reduction, Top. Catal. 57 (2013) 245–254. doi:10.1007/s11244-013-0179-y.

[46] M. Escudero-Escribano, A. Verdaguer-Casadevall, P. Malacrida, U. Grønbjerg, B.P. Knudsen, A.K. Jepsen, J. Rossmeisl, I.E.L. Stephens, I. Chorkendorff, Pt 5Gd as a highly active and stable catalyst for oxygen electroreduction, J. Am. Chem. Soc. 134 (2012) 16476–16479. doi:10.1021/ja306348d.

[47] U.G. Vej-Hansen, J. Rossmeisl, I.E.L. Stephens, J. Schiøtz, Correlation between diffusion barriers and

alloying energy in binary alloys, Phys. Chem. Chem. Phys. 18 (2016) 3302–3307. doi:10.1039/c5cp04694g.

[48] P. Malacrida, M. Escudero-Escribano, A. Verdaguer-Casadevall, I.E.L. Stephens, I. Chorkendorff, Enhanced activity and stability of Pt–La and Pt–Ce alloys for oxygen electroreduction: the elucidation of the active surface phase, J. Mater. Chem. A. 2 (2014) 4234. doi:10.1039/c3ta14574c.

[49] A. Velazquez-Palenzuela, F. Masini, A.F. Pedersen, M. Escudero-Escribano, D. Deiana, P. Malacrida, T.W. Hansen, D. Friebel, A. Nilsson, I.E.L. Stephens, I. Chorkendorff, The enhanced activity of mass-selected PtxGd nanoparticles for oxygen electroreduction, J. Catal. 328 (2015) 297–307. doi:10.1016/j.jcat.2014.12.012.

[50] P. Hernandez-Fernandez, F. Masini, D.N. McCarthy, C.E. Strebel, D. Friebel, D. Deiana, P. Malacrida, A. Nierhoff, A. Bodin, A.M. Wise, J.H. Nielsen, T.W. Hansen, A. Nilsson, I.E.L. Stephens, I. Chorkendorff, Mass-selected nanoparticles of PtxY as model catalysts for oxygen electroreduction, Nat. Chem. 6 (2014) 732–738. doi:10.1038/nchem.2001.

[51] R. Brandiele, C. Durante, E. Gradzka, G.A. Rizzi, J. Zheng, D. Badocco, P. Centomo, P. Pastore, G. Granozzi, A. Gennaro, One Step forward to a Scalable Synthesis of Platinum-Yttrium alloyed Nanoparticles on Mesoporous Carbon for Oxygen Reduction Reaction, J. Mater. Chem. A. 4 (2016) 12232–12240. doi:10.1039/C6TA04498K.

[52] A. Maljusch, J.B. Henry, W. Schuhmann, A.S. Bondarenko, A quick method for the preparation of Pt(111)-like thin films, Electrochem. Commun. 16 (2012) 88–91. doi:10.1016/j.elecom.2011.12.004.

[53] J.B. Henry, A. Maljusch, M. Huang, W. Schuhmann, A.S. Bondarenko, Thin-Film Cu − Pt(111) Near-Surface Alloys: Active Electrocatalysts for the Oxygen Reduction Reaction, ACS Catal. 2 (2012) 1457–1460. doi:10.1021/cs300165t.

[54] P.K. Sinha, W. Gu, A. Kongkanand, E. Thompson, Performance of Nano Structured Thin Film (NSTF) Electrodes under Partially-Humidified Conditions, J. Electrochem. Soc. 158 (2011) B831–B840. doi:10.1149/1.3590748.

[55] J. Kibsgaard, A. Jackson, T.F. Jaramillo, Mesoporous platinum nickel thin films with double gyroid morphology for the oxygen reduction reaction, Nano Energy. 29 (2016) 243–248. doi:10.1016/j.nanoen.2016.05.005.

[56] M. Inaba, T. Suzuki, T. Hatanaka, Y. Morimoto, Fabrication and Cell Analysis of a Pt/SiO2 Platinum Thin Film Electrode, J. Electrochem. Soc. 162 (2015) F634–F638. doi:10.1149/2.0201507jes.

[57] S.E. Temmel, E. Fabbri, D. Pergolesi, T. Lippert, T.J. Schmidt, Tuning the Surface Electrochemistry by Strained Epitaxial Pt Thin Film Model Electrodes Prepared by Pulsed Laser Deposition, Adv. Mater. Interfaces. 3 (2016) 1600222. doi:10.1002/admi.201600222.

[58] S.E. Temmel, E. Fabbri, D. Pergolesi, T.K. Lippert, T.J. Schmidt, Investigating the Role of Strain towards the Oxygen Reduction Activity on Model Thin Film Pt Catalysts, ACS Catal. 6 (2016) 7566–7576. doi:10.1021/acscatal.6b01836.

[59] S.J. Yoo, K.-S. Lee, S.J. Hwang, Y.-H. Cho, S.-K. Kim, J.W. Yun, Y.-E. Sung, T.-H. Lim, Pt3Y electrocatalyst for oxygen reduction reaction in proton exchange membrane fuel cells, Int. J. Hydrogen Energy. 37 (2012) 9758–9765. doi:10.1016/j.ijhydene.2012.03.089.

[60] S.J. Yoo, S.J. Hwang, J.-G. Lee, S.-C. Lee, T.-H. Lim, Y.-E. Sung, A. Wieckowski, S.-K. Kim, Promoting effects of La for improved oxygen reduction activity and high stability of Pt on Pt–La alloy electrodes, Energy Environ. Sci. 5 (2012) 7521–7525. doi:10.1039/c2ee02691k.

[61] S.J. Hwang, S.K. Kim, J.G. Lee, S.C. Lee, J.H. Jang, P. Kim, T.H. Lim, Y.E. Sung, S.J. Yoo, Role of electronic perturbation in stability and activity of Pt-based alloy nanocatalysts for oxygen reduction, J. Am. Chem. Soc. 134 (2012) 19508–19511. doi:10.1021/ja307951y.

[62] J. Snyder, N. Danilovic, A.P. Paulikas, D. Tripkovic, D. Strmcnik, N.M. Markovic, V.R. Stamenkovic, Thin film approach to single crystalline electrochemistry, J. Phys. Chem. C. 117 (2013) 23790–23796. doi:10.1021/jp4078272.

[63] J.R. O'Dea, M.E. Holtz, A.E. Legard, S.D. Young, R.G. Burns, A.R. Van Wassen, D.A. Muller, H.D. Abruña, F.J. DiSalvo, R.B. Van Dover, J.A. Marohn, Conductivity and Microstructure of Combinatorially Sputter-Deposited Ta-Ti-Al Nitride Thin Films, Chem. Mater. 27 (2015) 4515–4524. doi:10.1021/cm504599s.

[64] R. Frydendal, E.A. Paoli, I. Chorkendorff, J. Rossmeisl, I.E.L. Stephens, Toward an Active and Stable Catalyst for Oxygen Evolution in Acidic Media : Ti-Stabilized MnO2, 5 (2015) 1500991. doi:10.1002/aenm.201500991.

[65] K. Shinozaki, J.W. Zack, R.M. Richards, B.S. Pivovar, S.S. Kocha, Oxygen Reduction Reaction Measurements on Platinum Electrocatalysts Utilizing Rotating Disk Electrode Technique: I. Impact of Impurities, Measurement Protocols and Applied Corrections, J. Electrochem. Soc. 162 (2015) F1144–F1158. doi:10.1149/2.1071509jes.

[66] U.A. Paulus, A. Wokaun, G.G. Scherer, T.J. Schmidt, V. Stamenkovic, N.M. Markovic, P.N. Ross, Oxygen reduction on high surface area Pt-based alloy catalysts in comparison to well defined smooth bulk alloy electrodes, Electrochim. Acta. 47 (2002) 3787–3798. doi:10.1016/S0013-4686(02)00349-3.

[67] N.M. Marković, H. Gasteiger, P.N. Ross Jr., Oxygen Reduction on Platinum Low-Index Single-Crystal Surfaces in Sulfuric Acid Solution: Rotating Ring-Pt(hkl) Disk Studies, J. Phys. Chem. A. 99 (1995) 3411–3415.

[68] V. Climent, J.M. Feliu, Thirty years of platinum single crystal electrochemistry, J. Solid State Electrochem. 15 (2011) 1297–1315. doi:10.1007/s10008-011-1372-1.

[69] J. Clavilier, R. Faure, G. Guinet, R. Durand, Preparation of monocrystalline Pt microelectrodes and electrochemical study of the plane surfaces cut in the direction of the {111} and {110} planes, J. Electroanal. Chem. 107 (1979) 205–209. doi:10.1016/S0022-0728(79)80022-4.

[70] C.M. Pedersen, M. Escudero-Escribano, A. Velázquez-Palenzuela, L.H. Christensen, I. Chorkendorff, I.E.L. Stephens, Benchmarking Pt-based electrocatalysts for low temperature fuel cell reactions with the rotating disk electrode: oxygen reduction and hydrogen oxidation in the presence of CO (review article), Electrochim. Acta. 179 (2015) 647–657. doi:10.1016/j.electacta.2015.03.176.

[71] V. Kolic, J. Tymoczko, A. Maljusch, A. Ganassin, W. Schuhmann, A.S. Bandarenka, Experimental Aspects in Benchmarking of the Electrocatalytic Activity, ChemElectroChem. 2 (2015) 143–149. doi:10.1002/celc.201402295.

[72] K.J.J. Mayrhofer, D. Strmcnik, B.B. Blizanac, V. Stamenkovic, M. Arenz, N.M. Markovic, Measurement

of oxygen reduction activities via the rotating disc electrode method: From Pt model surfaces to carbon-supported high surface area catalysts, Electrochim. Acta. 53 (2008) 3181–3188. doi:10.1016/j.electacta.2007.11.057.

[73] S. Rudi, C. Cui, L. Gan, P. Strasser, Comparative Study of the Electrocatalytically Active Surface Areas (ECSAs) of Pt Alloy Nanoparticles Evaluated by Hupd and CO-stripping voltammetry, Electrocatalysis. 5 (2014) 408–418. doi:10.1007/s12678-014-0205-2.

[74] T. Biegler, D.A.J. Rand, R. Woods, Limiting oxygen coverage on platinized platinum; Relevance to determination of real platinum area by hydrogen adsorption, J. Electroanal. Chem. 29 (1971) 269–277. doi:10.1016/S0022-0728(71)80089-X.

[75] N.P. Lebedeva, M.T.M. Koper, J.M. Feliu, R.A. Van Santen, Role of crystalline defects in electrocatalysis: Mechanism and kinetics of CO adlayer oxidation on stepped platinum electrodes, J. Phys. Chem. B. 106 (2002) 12938–12947. doi:10.1021/jp0204105.

[76] G. García, M.T.M. Koper, Carbon monoxide oxidation on Pt single crystal electrodes: Understanding the catalysis for low temperature fuel cells, ChemPhysChem. 12 (2011) 2064–2072. doi:10.1002/cphc.201100247.

[77] U.S. Department of Energy, Energy Efficiency and Renewable Energy.

[78] Fuel Cell Commercialization Conference of Japan, Commercialization Scenario for FCVs and H2 Stations, ECS Trans. 41 (2010) 775–784.

[79] L. Dubau, F. Maillard, Unveiling the crucial role of temperature on the stability of oxygen reduction reaction electrocatalysts, Electrochem. Commun. 63 (2016) 65–69. doi:10.1016/j.elecom.2015.12.011.

[80] B. Predel, Phase Equilibria, Crystallographic and Thermodynamic Data of Binary Alloys, in: Landolt-Börnstein - Gr. IV Phys. Chem., 1996: p. 5F.

[81] M.J.T.C. Van Der Niet, N. Garcia-Araez, J. Hernández, J.M. Feliu, M.T.M. Koper, Water dissociation on well-defined platinum surfaces: The electrochemical perspective, Catal. Today. 202 (2013) 105–113. doi:10.1016/j.cattod.2012.04.059.

[82] E.H. Hoster, B.O. Alves, M.T.M. Koper, Tuning Adsorption via Strain and Vertical Ligand Effects, ChemPhysChem. 11 (2009) 1518–1524. doi: 10.1002/cphc.200900500

[83] D.F. Van Der Vliet, C. Wang, D. Li, A.P. Paulikas, J. Greeley, R.B. Rankin, D. Strmcnik, D. Tripkovic, N.M. Markovic, V.R. Stamenkovic, Unique electrochemical adsorption properties of Pt-skin surfaces, Angew. Chemie - Int. Ed. 51 (2012) 3139–3142. doi:10.1002/anie.201107668.

[84] A.F. Pedersen, E.T. Ulrikkeholm, M. Escudero-Escribano, T.P. Johansson, P. Malacrida, C.M. Pedersen, M.H. Hansen, K.D. Jensen, J. Rossmeisl, D. Friebel, A. Nilsson, I. Chorkendorff, I.E.L. Stephens, Probing the nanoscale structure of the catalytically active overlayer on Pt alloys with rare earths, Nano Energy. 29 (2016) 249–260. doi:10.1016/j.nanoen.2016.05.026.

[85] D.S. Strmcnik, D. V. Tripkovic, D. Van Der Vliet, K.C. Chang, V. Komanicky, H. You, G. Karapetrov, J.P. Greeley, V.R. Stamenkovic, N.M. Marković, Unique activity of platinum adislands in the CO electrooxidation reaction, J. Am. Chem. Soc. 130 (2008) 15332–15339. doi:10.1021/ja8032185.

[86] A. Verdaguer-Casadevall, C.W. Li, T.P. Johansson, S.B. Scott, J.T. McKeown, M. Kumar, I.E.L.

Stephens, M.W. Kanan, I. Chorkendorff, Probing the Active Surface Sites for CO Reduction on Oxide-Derived Copper Electrocatalysts, J. Am. Chem. Soc. 137 (2015) 9808–9811. doi:10.1021/jacs.5b06227.

[87] A. López-Cudero, Á. Cuesta, C. Gutiérrez, Potential dependence of the saturation CO coverage of Pt electrodes: The origin of the pre-peak in CO-stripping voltammograms. Part 1: Pt(111), J. Electroanal. Chem. 579 (2005) 1–12. doi: 10.1016/j.jelechem.2005.01.018

[88] M.J. Weaver, S.C. Chang, L.W.H. Leung, X. Jiang, M. Rubel, M. Szklarczyk, D. Zurawski, A. Wieckowski, Evaluation of absolute saturation coverages of carbon monoxide on ordered low-index platinum and rhodium electrodes, J. Electroanal. Chem. 327 (1992) 247–260. doi:10.1016/0022-0728(92)80151-S.

[89] D.N. McCarthy, C.E. Strebel, T.P. Johansson, A. den Dunnen, A. Nierhoff, J.H. Nielsen, I. Chorkendorff, Structural Modification of Platinum Model Systems under High Pressure CO Annealing, J. Phys. Chem. C. 116 (2012) 15353–15360. doi:10.1021/jp302379x.

[90] Q.S. Chen, J. Solla-Gullón, S.G. Sun, J.M. Feliu, The potential of zero total charge of Pt nanoparticles and polycrystalline electrodes with different surface structure: The role of anion adsorption in fundamental electrocatalysis, Electrochim. Acta. 55 (2010) 7982–7994. doi:10.1016/j.electacta.2010.03.050.

[91] J. Solla-Gullón, P. Rodríguez, E. Herrero, A. Aldaz, J.M. Feliu, Surface characterization of platinum electrodes., Phys. Chem. Chem. Phys. 10 (2008) 1359–1373. doi:10.1039/b709809j.

[92] F.J. Vidal-Iglesias, R.M. Arán-Ais, J. Solla-Gullón, E. Herrero, J.M. Feliu, Electrochemical Characterization of Shape-Controlled Pt Nanoparticles in Different Supporting Electrolytes, ACS Catal. 2 (2012) 901–910. doi:dx.doi.org/10.1021/cs200681x.

[93] A. Cuesta, A. Couto, A. Rincón, M.C. Pérez, A. López-Cudero, C. Gutiérrez, Potential dependence of the saturation CO coverage of Pt electrodes: The origin of the pre-peak in CO-stripping voltammograms. Part 3: Pt(poly), J. Electroanal. Chem. 586 (2006) 184–195. doi:10.1016/j.jelechem.2005.10.006.

[94] J.A. Bard, L.R. Faulkner, Electrochemical Methods: Fundamentals and Applications, 2nd Edition, 2001.

[95] F. Calle-Vallejo, M.T.M. Koper, A.S. Bandarenka, Tailoring the catalytic activity of electrodes with monolayer amounts of foreign metals., Chem. Soc. Rev. 42 (2013) 5210–30. doi:10.1039/c3cs60026b.